Development of the Stria Vascularis and Potassium Regulation in the Human Fetal Cochlea: Insights into Hereditary Sensorineural Hearing Loss

Heiko Locher,[1,2] John C.M.J. de Groot,[2] Liesbeth van Iperen,[1] Margriet A. Huisman,[2] Johan H.M. Frijns,[2] Susana M. Chuva de Sousa Lopes[1,3]

[1] Department of Anatomy and Embryology, Leiden University Medical Center, Leiden, 2333 ZA, the Netherlands

[2] Department of Otorhinolaryngology and Head and Neck Surgery, Leiden University Medical Center, Leiden, 2333 ZA, the Netherlands

[3] Department for Reproductive Medicine, Ghent University Hospital, 9000 Ghent, Belgium

Received 25 August 2014; revised 2 February 2015; accepted 2 February 2015

ABSTRACT: **Sensorineural hearing loss (SNHL) is one of the most common congenital disorders in humans, afflicting one in every thousand newborns. The majority is of heritable origin and can be divided in syndromic and nonsyndromic forms. Knowledge of the expression profile of affected genes in the human fetal cochlea is limited, and as many of the gene mutations causing SNHL likely affect the stria vascularis or cochlear potassium homeostasis (both essential to hearing), a better insight into the embryological development of this organ is needed to understand SNHL etiologies. We present an investigation on the development of the stria vascularis in the human fetal cochlea between 9 and 18 weeks of gestation (W9–W18) and show the cochlear expression dynamics of key potassium-regulating proteins. At W12, MITF+/SOX10+/KIT+ neural-crest-derived melanocytes migrated into the cochlea and penetrated the basement membrane of the lateral wall epithelium, developing into the intermediate cells of the stria vascularis. These melanocytes tightly integrated with Na^+/K^+-ATPase-positive marginal cells, which started to express KCNQ1 in their apical membrane at W16. At W18, KCNJ10 and gap junction proteins GJB2/CX26 and GJB6/CX30 were expressed in the cells in the outer sulcus, but not in the spiral ligament. Finally, we investigated GJA1/CX43 and GJE1/CX23 expression, and suggest that GJE1 presents a potential new SNHL associated locus. Our study helps to better understand human cochlear development, provides more insight into multiple forms of hereditary SNHL, and suggests that human hearing does not commence before the third trimester of pregnancy.** © 2015 Wiley Periodicals, Inc. Develop Neurobiol 75: 1219–1240, 2015

Keywords: **human; sensorineural hearing loss; development; stria vascularis; melanocytes**

INTRODUCTION

According to recent estimates of the World Health Organization, more than 5% of the world's total population suffer from some form of disabling hearing loss (WHO, 2014). A large part of this hearing loss is of sensorineural nature, making sensorineural hearing

Correspondence to: H. Locher (h.locher@lumc.nl) or S. M. Chuva de Sousa Lopes (lopes@lumc.nl)

Contract grant sponsor: Netherlands Organisation for Scientific Research (NWO, ASPASIA 015.007.037, www.nwo.nl/aspasia.

Contract grant sponsor: Interuniversity Attraction Poles (IAP, P7/07).

Contract grant sponsor: Stichting Het Heinsius-Houbolt Fonds, the Netherlands (to H.L.).

Additional Supporting Information may be found in the online version of this article.

Published online 28 February 2015 in Wiley Online Library (wileyonlinelibrary.com).

DOI 10.1002/dneu.22279

loss (SNHL) the most prevalent sensorineural disorder in humans. SNHL is also the most common congenital disorder, with a prevalence of 1 in every 1000 newborns in the UK and the Netherlands (with a bilateral hearing loss $\geq$ 40 dB (NHSP, 2011; van der Ploeg et al., 2012)). Of these, over two-thirds can be attributed to genetic factors. Hereditary SNHL can be classified in syndromic ($\sim$25%) and nonsyndromic ($\sim$75%) forms (Morton and Nance, 2006).

Examples of syndromic SNHL include Pendred's syndrome ([MIM 274600, www.omim.org/], combining hearing loss and goiter (Pendred, 1896; Bizhanova and Kopp, 2010)), Waardenburg syndrome [WS; hearing loss and pigmentation abnormalities (Waardenburg, 1951; Pingault et al., 2010)] and Jervell and Lange-Nielsen syndrome ([MIM 220400 and MIM 612347], hearing loss and cardiac symptoms (Jervell and Lange-Nielsen, 1957)). In nonsyndromic SNHL, associations with obvious abnormalities of the external ear or symptoms other than hearing loss cannot be found, but the heterogeneity of loci and genes is high: over 130 loci have been mapped and over 60 different genes have been implicated presently (van Camp and Smith). Nonsyndromic forms are grouped in autosomal dominant (DFNA), autosomal recessive (DFNB), X-linked (DNFX) and mitrochondrial subtypes. The most commonly affected gene causing nonsyndromic hearing loss (both in autosomal recessive DFNB1A [MIM 220290] and in autosomal dominant DFNA3A [MIM 601544]) is gap junction beta 2 (*GJB2*, [MIM 121011]), the gene encoding the connexin 26 protein (CX26) (Kelsell et al., 1997; Denoyelle et al., 1997). Depending on the studied population, 20–50% of all recessive nonsyndromic SNHL cases can be attributed to a mutation in *GJB2* (Hilgert et al., 2009a; Linden Phillips et al., 2013). For a comprehensive overview of other affected genes, we refer to recent reviews (Hilgert et al., 2009b; Angeli et al., 2012; Shearer and Smith, 2012; Smith et al., 2014; Stelma and Bhutta, 2014).

In SNHL, the disorder lies either in the cochlea itself or in any of the retrocochlear auditory structures. Cochlear hair cells are responsible for converting sound into electrical signals that travel to the brainstem via the cochlear nerve (Hudspeth, 1989). Hair cell function depends on the endocochlear potential, a positive extracellular potential ($\approx$80–100 mV relative to perilymph) in the endolymph of the cochlear duct (or scala media), generated by an unusually high concentration of potassium ions (K^+) (Smith et al., 1954). These ions are secreted into the endolymph by specialized cells within the stria vascularis, located in the lateral wall of the cochlear duct (Patuzzi, 2011). The stria vascularis is highly vascularized and consists of three layers of distinct cell types: the marginal cells, the intermediate cells (melanocytes), and the basal cells (Kimura and Schuknecht, 1970; Hilding and Ginzberg, 1977). It is generally accepted that the depolarizing K^+ flow causing hair cell activation in the organ of Corti is recycled back to the stria vascularis via the epithelial lining of the cochlear duct and the spiral ligament fibrocytes, and/or through the perilymph, as depicted in Figure 1. To maintain the endocochlear potential, this recycling system requires a specific distribution of cochlear cell types as well as selective ion channels and gap-junctions (Zdebik et al., 2009; Adachi et al., 2013).

Therefore, it is not surprising that many gene mutations causing SNHL either result in functional changes of the ion channels involved in K^+ homeostasis or cause an abnormal cellular morphology in the cochlea. Although progress has been made in identifying the genes responsible for SNHL in humans, knowledge on their actual expression in the human cochlea is limited and only a few studies have investigated the morphological development of the stria vascularis in the human fetal cochlea (Lavigne-Rebillard and Bagger-Sjöbäck, 1992; Bibas et al., 2000). In this article, we address both aspects, focussing on the embryonic development of the lateral wall in the human fetal cochlea. We show the expression profiles of several genes involved in syndromic and nonsyndromic SNHL (Table 1) between 9 and 18 weeks of gestation (W9–W18). More specifically, we have investigated the development of the different cell types in the stria vascularis and studied the expression of K^+-regulating and gap junction proteins. Together, our data give insight in hereditary SNHL and provide a basis for K^+-recycling models in the human cochlea.

METHODS

Tissue Samples

Human fetal cochleas were collected from tissues obtained by elective abortion (healthy subjects, no medical indication) using vacuum aspiration. Prior to the procedure, obstetric ultrasonography was used to determine the gestational age in weeks and days. Of all collected cochleas, we discarded those which where mechanically damaged or showed marked tissue degeneration, upon inspection by light-microscopy. Cochleas of the following gestational ages were collected and used: W9, W9.1, W10.4 (2×), W12 (2×), W12.2, W14 (2×), W16 (2×), W18 (3×). The cochleas were obtained in PBS, fixed in 4% paraformaldehyde in PBS overnight at 4°C, decalcified and embedded in paraffin as previously described (Locher et al., 2013). The

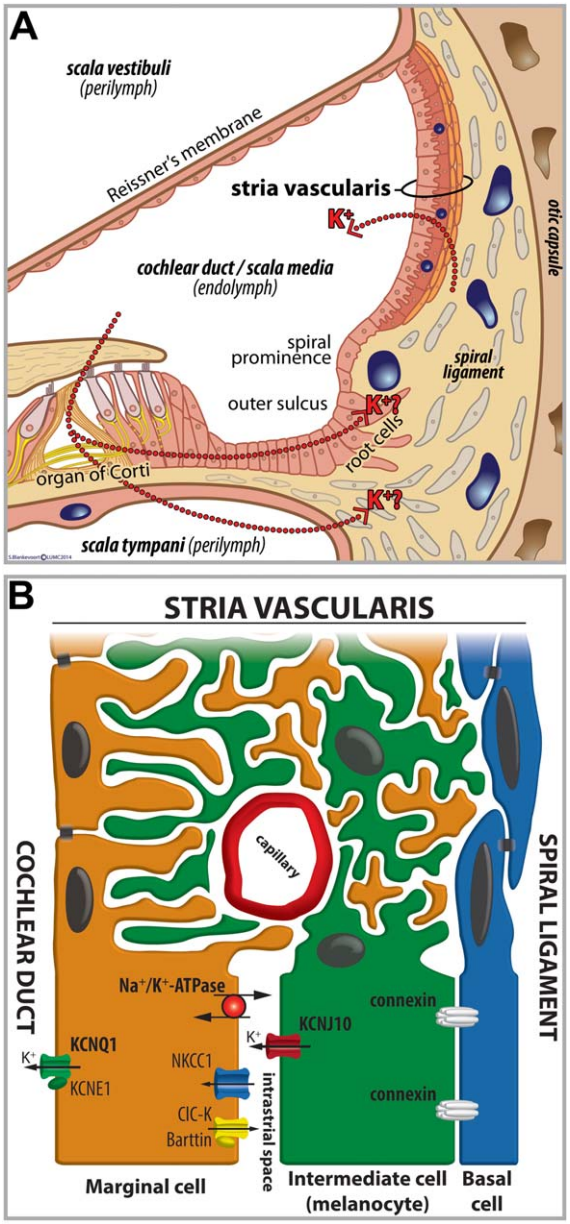

Figure 1 Capturing cochlear potassium homeostasis in mammals. (A) A schematic illustration of a cross-section through the adult cochlea. The cochlear duct (or scala media) is filled with endolymph containing a high [K^+] that is maintained by the stria vascularis. Potassium recycling is postulated to either occur via the supporting cells of the organ of Corti and the epithelial lining of the outer sulcus (Claudius cells and root cells), or through the perilymph of the scala tympani. (B) A schematic anatomical (upper half) and compartmental (lower half) model of the adult stria vascularis showing the three cellular layers and depicting the location of potassium regulating channels. The stria vascularis is electrochemically isolated from neighboring structures by tight junctions (black bars). [Color figure can be viewed in the online issue, which is available at wileyonlinelibrary.com.]

use of human fetal material was approved by the Medical Ethical Committee of the Leiden University Medical Center (protocol 08.087). Informed written consent was obtained in accordance with the WMA Declaration of Helsinki guidelines.

Immunohistochemistry

The cochleas were cut in 5 or 10 μm thick sections in the sagittal plane using a RM2255 microtome (Leica). Deparaffinization and immunohistochemistry were carried out as previously described (Locher et al., 2013). Briefly, antigen retrieval was performed (see below) and sections were consecutively incubated with primary and secondary antibodies diluted in blocking solution consisting of 1% bovine serum albumin (Sigma-Aldrich) and 0.05% Tween-20 (Promega) in PBS. Nuclei were stained with 4′,6-diamidino-2-phenylindole (DAPI, Vector Laboratories). The primary antibodies used in this study were mouse anti-acetylated tubulin (aceTUBA, 1:500, T6793, Sigma), rabbit anti-collagen type IV (COL4, 1:200, AB748, Chemicon), rabbit anti-fibronectin (FN, 1:400, F3648, Sigma-Aldrich), rabbit anti-GJA1 (1:1000, C6219, Sigma), rabbit anti-GJA1 (1:2000, ACC-201, Alomone labs), rabbit anti-GJB2 (1:100, ACC-212, Alomone labs), rabbit anti-GJB6 (1:100, PA511640, Thermo Scientific), rabbit anti-GJE1 (1:1000, NBP2–14051, Novus biologicals), goat anti-KCNJ10 (1:100, NBP1–70371), rabbit anti-KCNQ1 (1:200, ab65092, Abcam), rabbit anti-KCNQ1 (1:100, APC-022, Alomone labs), rabbit anti-KIT (1:100, A4502, Dako), rabbit anti-laminin (LAM, 1:200, Z009701, Dako), rabbit anti-melan-A (1:500, NBP1–30151, Novus), mouse anti-microphthalmia-associated transcription factor (MITF, 1:100, M3621, Dako), mouse anti-Na^+/K^+-ATPase α1 (ATP1A1, 1:200, α6F, Developmental Studies Hybridoma Bank), rabbit anti-solute family carrier 2, member 1 (SLC2A1, 1:500, ab15309, Abcam), and goat anti-SOX10 (1:50, sc-17342, Santa Cruz Biotechnology). Prior to immunostaining for COL4, LAM, and FN antibodies, antigen retrieval was performed by incubating sections for 5 min with 20 µg/mL proteinase K (Promega) in Tris-EDTA-$CaCl_2$ buffer (pH8.0). In all other cases, tissue sections were treated for 12 min at 97°C with 0.01 *M* sodium citrate buffer (pH 6.0) and allowed to cool down. The secondary antibodies used were Alexa Fluor (AF) conjugated immunoglobulins (Life Technologies): AF 488 donkey anti-mouse (A-21202), AF 488 donkey anti-rabbit (A-21206), AF 488 donkey anti-goat (A-11055), AF 568 donkey anti-mouse (A-10037), and AF 568 donkey anti-rabbit (A-10042), all at a 1:500 dilution. As antibody specificity controls, primary antibodies were routinely omitted (negative control), isotype controls were performed (negative control), and immunostainings were performed on adult mouse cochlea (positive control). On human fetal tissue, at least three separate immunostaining experiments were performed with each primary antibody. To further verify specificity, all immunostaining results were checked to confirm the appropriate cellular location of the fluorescent signals

Table 1 Selected Genes and Association with Syndromic and Nonsyndromic Sensorineural Hearing Loss

Gene	MIM	SNHL in Genetic Disorder *(MIM)*
MITF	156845	Waardenburg syndrome, type 2A *(193510)*
		Waardenburg syndrome/ocular albinism, digenic *(103470)*
		Tietz albinism-deafness syndrome *(103500)*
SOX10	602229	Waardenburg syndrome, type 4C *(613266)*
		Waardenburg syndrome, type 2E *(611584)*
		PCWH syndrome *(609136)*
		Kallman syndrome with deafness *(not defined)*
KIT	164920	Piebaldism *(172800)*
KCNQ1 (KVLQT1)	607542	Jervell and Lange-Nielsen syndrome *(220400)*
KCNJ10 (K_{ir}4.1)	602208	Enlarged vestibular aqueduct, digenic *(600791)*
		SESAME syndrome *(612780)*
GJB2 (CX26)	121011	DFNA3A *(601544)*
		DFNB1A *(220290)*
		Hystrix-like ichthyosis with deafness *(602540)*
		Keratitis-ichthyosis-deafness syndrome *(148210)*
		Bart-Pumphrey syndrome *(149200)*
		Keratoderma, palmoplantar, with deafness *(148350)*
		Vohwinkel syndrome *(124500)*
GJB6 (CX30)	604418	DFNA3B *(612643)*
		DFNB1B *(612645)*
		DFNB1A, digenic *(220290)*
GJA1 (CX43)	121014	DFN not defined
GJE1 (CX23)	Not defined	Unknown

and tissue expression patterns were compared to previous studies using experimental animals, if available.

Image Acquisition and Processing

Confocal images were acquired with a Leica SP8 confocal laser scanning microscope operating under the Leica Application Suite Advanced Fluorescence software (LAS AF) using Leica objectives (40×/1.3 oil HC PL Apo or 63×/1.4 oil HC PL Apo). Maximal projections were obtained from image stacks with a z-step size of 0.5 μm. Brightness and contrast adjustments consistent with image manipulation policies were performed either with LAS AF, Fiji (ImageJ version 1.48k (Schindelin et al., 2012)) or Adobe Photoshop CS6 (Adobe Systems) image-processing software.

RESULTS

Melanocytes Invade the Lateral Wall Epithelium at W12 and Develop into the Intermediate Cells

The cochlear melanocytes that form the intermediate cell layer of the stria vascularis are thought to originate from the neural crest. To investigate the formation of the three cell layers of the stria vascularis, we first determined the cochlear location of melanocytes and monitored their invasion into the lateral wall epithelium during embryonic development of the human fetal cochlea. Immunostaining for melan-A ([MIM 605313], a marker of melanocytes) and acetylated α-tubulin (aceTUBA, which labels various types of epithelial and neural cells) allowed us to visualize melanocyte location and general cochlear architecture. At W9.1, the melan-A+ melanocytes were located both in the part of the periotic mesenchyme that will develop into the otic capsule (called hereafter: otic capsule), and in the part of the periotic mesenchyme that will form the spiral ligament and the spiral limbus (called hereafter: periotic mesenchyme) but not in the epithelium of the cochlear duct [Fig. 2(A,B), Supporting Information Figure S1]. More specifically, most melanocytes were found in the apical half of the developing cochlea situated above the cochlear duct, and only a few could be observed in the periotic mesenchyme bordering the lateral wall epithelium, that is, the future stria vascularis [Fig. 2(B), right arrowhead]. Immunostaining for basement membrane proteins LAM (Supporting Information Figure S2A), COL4 (Supporting Information Figure S2B), and FN (Supporting Information Figure S2C) at W9.4 showed a strictly continuous and smooth basement membrane, further confirming the mesenchymal location of the melanocytes. At W10.4, the cochlear duct

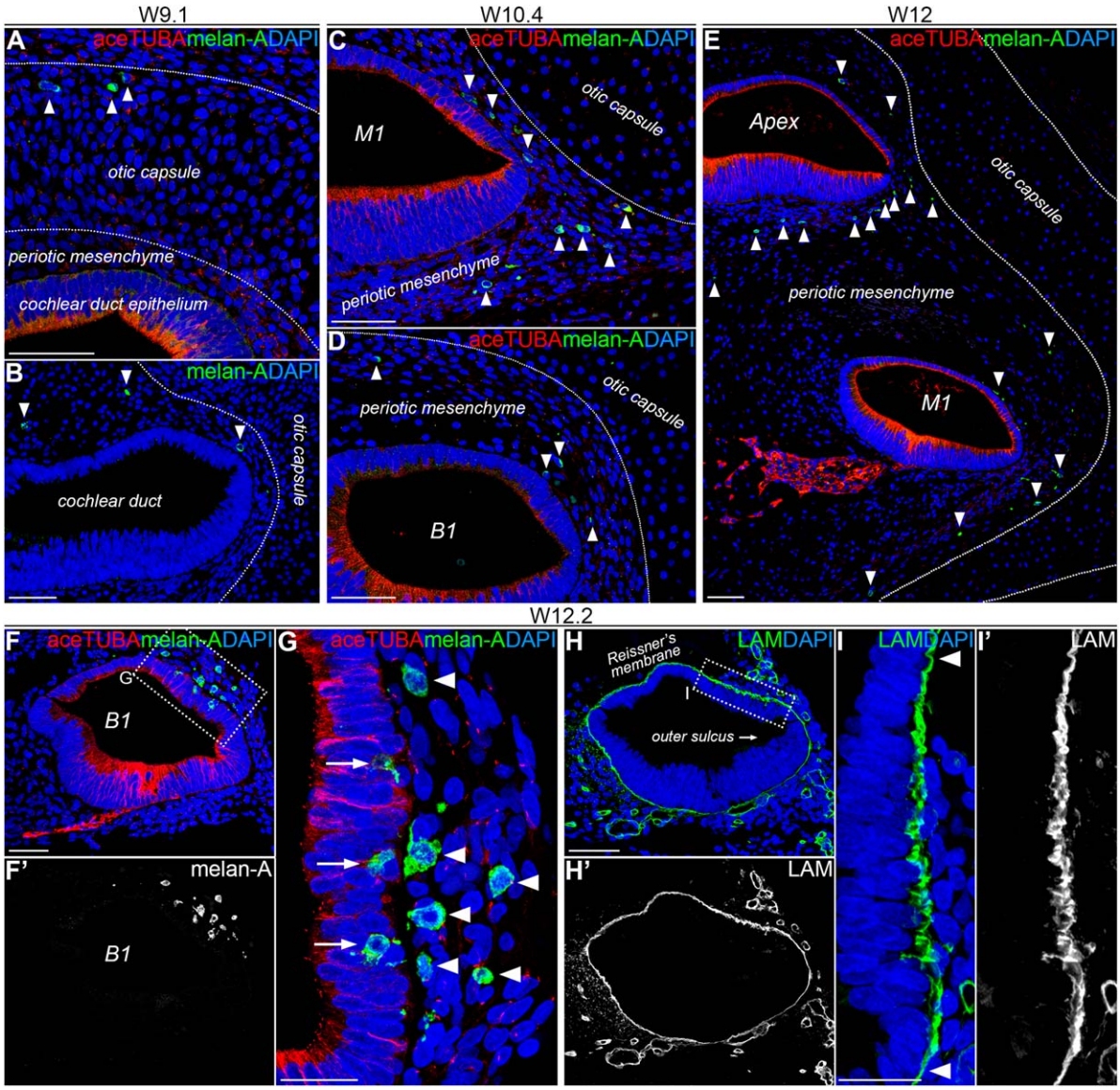

Figure 2 Migration of melanocytes into the stria vascularis of the human fetal cochlea. (A-B) A cochlea at W9.1 immunostained for acetylated tubulin (aceTUBA; red), melan-A (green) and DAPI (blue) (A) or melan-A (green) and DAPI (blue) (B). Arrowheads point to melan-A+ cochlear melanocytes. Scale bars = 50 μm. (C) The lower middle turn (M1) of a cochlea at W10.4 immunostained for aceTUBA (red), melan-A (green), and DAPI (blue). Scale bar = 50 μm. (D) The lower basal turn (B1) of a cochlea at W10.4 immunostained for aceTUBA (red), melan-A (green), and DAPI (blue). Scale bar = 50 μm. (E) The apical and lower middle turn of cochlea at W12 immunostained for aceTUBA (red), melan-A (green), and DAPI (blue). Scale bar = 50 μm. (F-F′) The lower basal turn of a cochlea at W12.2 immunostained for aceTUBA (red), melan-A (green), and DAPI (blue). The melan-A signal is shown separately in white in (F′). Scale bar = 50 μm. (G). Higher magnification of the outlined area in (F). Arrowheads point to melan-A+ melanocytes located in the periotic mesenchyme. Arrows point to melan-A+ melanocytes located in between the epithelial lining of the cochlear duct lateral wall (the future marginal cells of the stria vascularis). Scale bar = 20 μm. (H-H′). A similar section of the lower basal turn of a cochlea at W12.2 as depicted in (F), here immunostained for basement membrane protein laminin (LAM). The LAM signal is shown separately in white in (H′). Scale bar = 50 μm. (I-I′) Higher magnification of the developing stria vascularis outlined in (H). The arrowheads point to the smooth and continuous appearance of the basement membrane at the location of the bordering Reissner's membrane and the outer sulcus, as opposed to the irregular pattern observed in at the location of the future stria vascularis. The LAM signal is shown separately in white in (I′) Scale bar = 20 μm. [Color figure can be viewed in the online issue, which is available at wileyonlinelibrary.com.]

had spiralled twice around the central axis of the cochlea and melan-A+ melanocytes were observed exclusively in the periotic mesenchyme of the future middle and basal turns [Fig. 2(C,D), arrowheads]. When compared to W9.1, more melanocytes were located close to the lateral wall epithelium.

At W12, melan-A+ melanocytes were observed in all cochlear turns. In the apical and middle turns, melanocytes were still located exclusively to the periotic mesenchyme [Fig. 2(E)]. However, in the basal turn, melanocytes were observed both in the periotic mesenchyme [Fig. 2(F) and arrowheads in Fig. 2(G)] and in the lateral wall epithelium of the cochlear duct (the future stria vascularis), indicating that they had penetrated through the basement membrane [arrows in Fig. 2(G)]. This finding is in agreement with the observation that the basement membrane at this location showed irregular staining patterns for LAM, COL4, and FN, in contrast to its smooth and continuous appearance near the developing Reissner's membrane and at the location of the outer sulcus [Fig. 2(H,I) and three-dimensional reconstruction provided in Interactive PDF file 1].

Melanocytes in the Stria Vascularis Express MITF, SOX10, and KIT

Next, we investigated the expression of two genes, *MITF* [MIM 156845] and *SOX10* [MIM 602229] that are expressed in the melanocytic lineage. At W12, MITF was expressed in all turns in both the melan-A+ melanocytes in the periotic mesenchyme and in the melanocytes that had invaded the developing stria vascularis [Fig. 3(A)]. Previously, we have shown that SOX10+ cells are present in the spiral ganglion and throughout the cochlear epithelium (Locher et al., 2014). In this study, we also detected SOX10 expression in the presumptive melanocytes bordering the stria vascularis [Fig. 3(B), arrowheads].

Double immunostaining for MITF and KIT [MIM 164920], the latter protein being expressed in both the neural crest and the melanocytic lineage, at W12 showed that KIT was expressed by all MITF+ melanocytes [Fig. 3(C)]. In addition, KIT expression was found in the cochlear duct epithelium, in a few remaining mesenchymal cells within the developing scala tympani [Fig. 3(C,D)], and in the spiral ganglion (data not shown).

In the Developing Stria Vascularis, Melanocytes Integrate with the Marginal Cells in a Spatiotemporal Order

At W12, we detected a clear spatial gradient in the location of melanocytes, with epithelial invasion commencing in the basal turn [Fig. 2(E,F)]. To monitor this development, we immunostained cochleas at W14, W16, and W18 for melan-A and aceTUBA. At W14, melan-A+ melanocytes were still confined to the periotic mesenchyme in both the upper middle (M2) and lower middle (M1) turns [Fig. 4(A,B)]. In the upper basal turn (B2), melanocytes were observed invading the lateral wall epithelium [Fig. 4(C)] and in the lower basal turn (B1) most melanocytes were found integrating with the developing marginal cells [Fig. 4(D)]. At W16, integrating melanocytes were found in greater numbers and observed throughout all turns [Fig. 4(E–H)]. In addition to melanocytes in or near the lateral wall epithelium, we also consistently observed the presence of melan-A+ melanocytes along the edges of the otic capsule, here shown in the M2 turn at W16 [Fig. 4(I), arrowheads] and the B1 turn at W18 [Fig. 4(J), arrowheads]. At W18, melanocytes were found tightly integrated with the developing marginal cells in the B1 turn, and some melanocyte processes were also observed around the developing strial capillaries [Fig. 4(K), arrowheads]. Expression patterns of aceTUBA [Fig. 4(K)] and the basement membrane proteins LAM, COL4, and FN better accentuated the development of other regions in the lateral wall epithelium [Fig. 4(L–N), Supporting Information Figure S2D-L and Supporting Information Figure S3, and three-dimensional reconstruction provided in Interactive PDF files 2 and 3]. In particular, with these immunostainings the spiral prominence is clearly emerging, thereby demarcating the stria vascularis from the future root cells in the outer at W18.

Until W18, SLC2A1+ Basal Cells Were Not Detected in the Stria Vascularis

In the stria vascularis, in addition to the marginal cells and the melanocytes, we also investigated the formation of the third and innermost strial layer, that is, the basal cells. However, until W18, we were unable to detect any basal cells by immunostaining for solute family carrier 2, member 1 (SLC2A1, also known as GLUT1, [MIM 138140]), a glucose transporter known to be expressed by the rodent cochlear basal cells and vascular endothelial cells (Ito et al., 1993). SLC2A1 expression was found in the developing human stria vascularis but this expression was confined to capillaries and erythrocytes (Supporting Information Figure S4). Interestingly, we did observe consistent expression of SLC2A1 on the apical (luminal) membranes of all epithelial cells between the organ of Corti and the spiral prominence (Hensen's cells in the organ of Corti as well as Claudius' cells and root cells in the outer

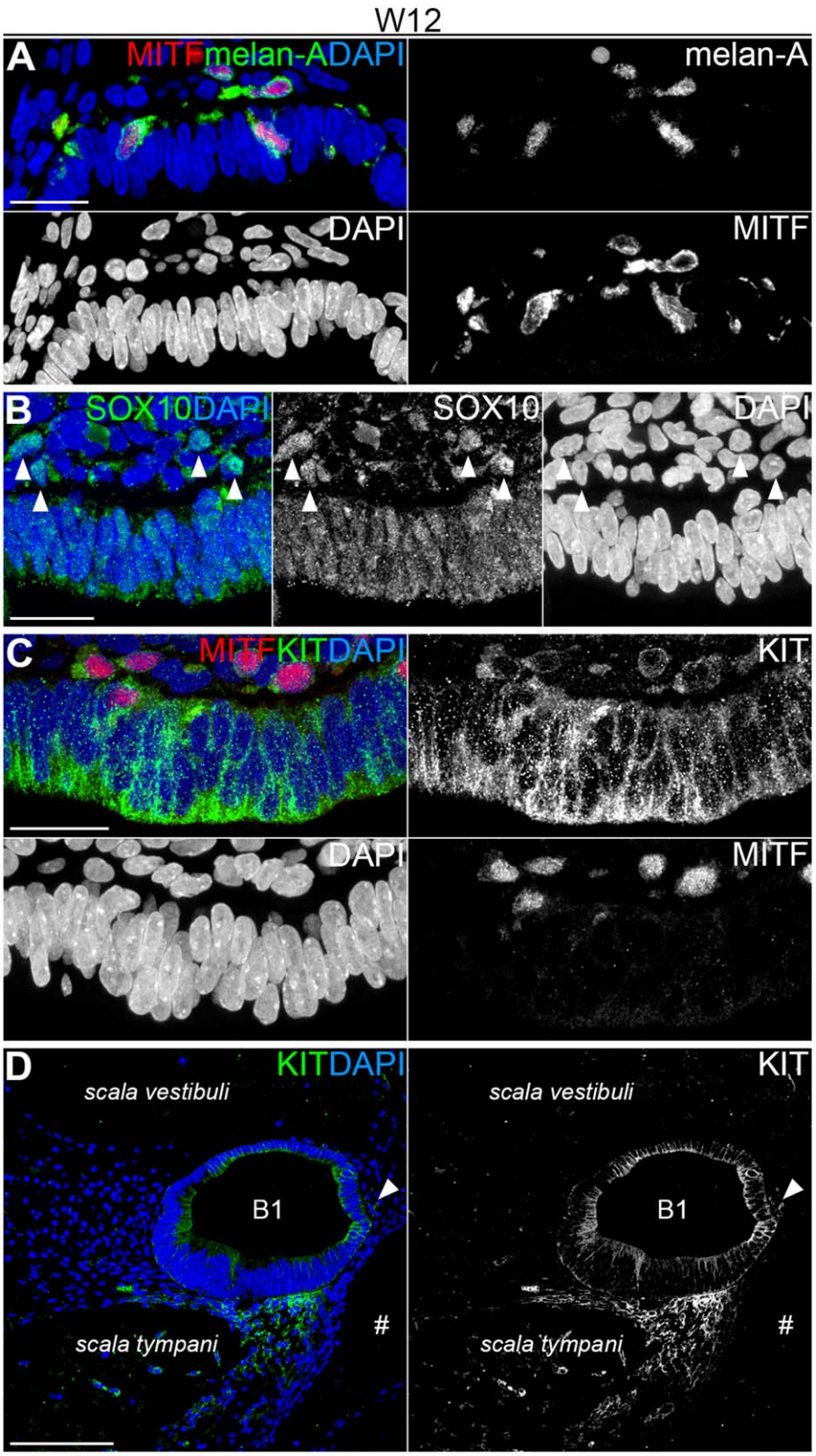
W12
A
MITFmelan-ADAPI
melan-A
DAPI
MITF
B
SOX10DAPI
SOX10
DAPI
C
MITFKITDAPI
KIT
DAPI
MITF
D
KITDAPI
scala vestibuli
B1
scala tympani
#
KIT
scala vestibuli
B1
scala tympani
#

sulcus) at all studied stages (from W12 to W18, Supporting Information Figure S4).

Dynamics of KCNQ1 in the Developing Human Cochlear Duct

To investigate the onset of expression and developmental distribution of ion channels and enzymes involved in cochlear K^+ transport and the generation of the endocochlear potential, we immunostained for the K^+ channel protein KCNQ1 [MIM 607542]. At W10.4 [Fig. 5(A)] and W12.2 [Fig. 5(B)], reactivity was observed at the basement membrane delineating the lateral wall epithelium. At W14, this pattern had changed to reactivity in the developing Reissner's membrane [arrowhead in Fig. 5(C)] and the future outer sulcus [arrow in Fig. 5(C)]. From W16 [Fig. 5(D,F)] to W18 [Fig. 5(H,I)] increased KCNQ1 expression was observed at the apical (luminal) membrane of the developing marginal cells in the stria vascularis, in addition to reactivity in Reissner's membrane [Fig. 5(E,H)] and the future root cells of the outer sulcus [Fig. 5(G,J)]. However, a different anti-KCNQ1 antibody clone (Alomone) that also recognizes the C-terminus of KCNQ1 did not show any reactivity in Reissner's membrane or in the root cells of the outer sulcus. It did, however, show identical reactivity in the developing marginal cells at W16 and W18 (data not shown). Although we cannot explain this difference as both antibodies should recognize the same KCNQ1 transcript, expression of KCNQ1 in Reissner's membrane has been reported previously (Kim et al., 2009).

Dynamics of Na^+/K^-–ATPase in the Developing Cochlear Duct

Already at W10.4, immunostaining for the alpha-1 subunit of Na^+/K^+-ATPase (ATP1A1, [MIM 182310]) was observed in different degrees throughout the entire epithelium of the cochlear duct, with a moderate intensity in the future stria vascularis [Fig. 6(A)]. However, at W12 ATP1A1 expression increased in the developing stria vascularis on the basolateral membranes of the developing marginal cells [Fig. 6(B)]. At W14 and W16, ATPA1 expression became even more prominent and was located in cells adjacent to the increasing numbers of invading melan-A+ melanocytes [Fig. 6(C–E)]. Immunostaining diminished in most parts of the epithelium, and at W18 ATP1A1 expression was found on the basolateral membranes of the marginal cells, on the basolateral membranes of the developing hair cells in the organ of Corti, as well as on both the apical and basolateral membranes of the Claudius' cells and the root cells in the outer sulcus [Fig. 6(F–H)]. Curiously, at this stage, pillar cells in the organ of Corti were also consistently found to stain positive for melan-A in the basal turn, although these are not of melanocytic origin [Fig. 6(G)]. Focusing on the stria vascularis, we found melan-A+ melanocyte processes penetrating between the marginal cells toward the lumen of the cochlear duct [Fig. 6(I), arrow]. We also observed ATP1A1 expression around the melan-A+ melanocyte cell bodies [Fig. 6(I), arrowhead] and around melanocyte processes encircling the strial capillaries [Fig. 6(J), arrows].

KCNJ10 Expression Is Confined to the Outer Sulcus at W18

From W16 onward, we observed KCNJ10 in the future root cells cells of the outer sulcus (Fig. 7). However, we did not observe KCNJ10 expression by strial melanocytes at any of the investigated stages (data not shown).

Distribution of GJB2, GJB6, GJA1, and GJE1 in the Human Fetal Cochlea

To investigated the developmental expression of gap junction proteins, we immunostained for GJB2 (CX26),

Figure 3 Expression of MITF, SOX10 and KIT. (A) Lateral wall area of the lower basal turn of a cochlea at W12 immunostained for microphthalmia-associated transcription factor (MITF) (red), melan-A (green), and DAPI (blue), showing Melan-A+/MITF+ melanocytes in the periotic mesenchyme as well as in the developing stria vascularis. Signals are shown separately in white. Scale bar = 20 μm. (B) Lateral wall area of the lower basal turn of a cochlea at W12 immunostained for SOX10 (green) and DAPI (blue). Signals are shown separately in white. Arrowheads point to SOX10+ melanocytes located in the periotic mesenchyme. Scale bar = 20 μm. (C) Lateral wall area of the lower basal turn of a cochlea at W12 immunostained for MITF (red), KIT (green), and DAPI (blue), showing KIT+/MITF+ melanocytes in the periotic mesenchyme as well as in the developing stria vascularis. Signals are shown separately in white. Scale bar = 100 μm. (D) The lower basal turn of a cochlea at W12 immunostained for KIT (green) and DAPI (blue). The KIT signal is shown separately in white. The arrowhead points to KIT+ melanocytes in the periotic mesenchyme next to the developing stria vascularis. # = Tissue artifact. Scale bar = 20 μm. [Color figure can be viewed in the online issue, which is available at wileyonlinelibrary.com.]

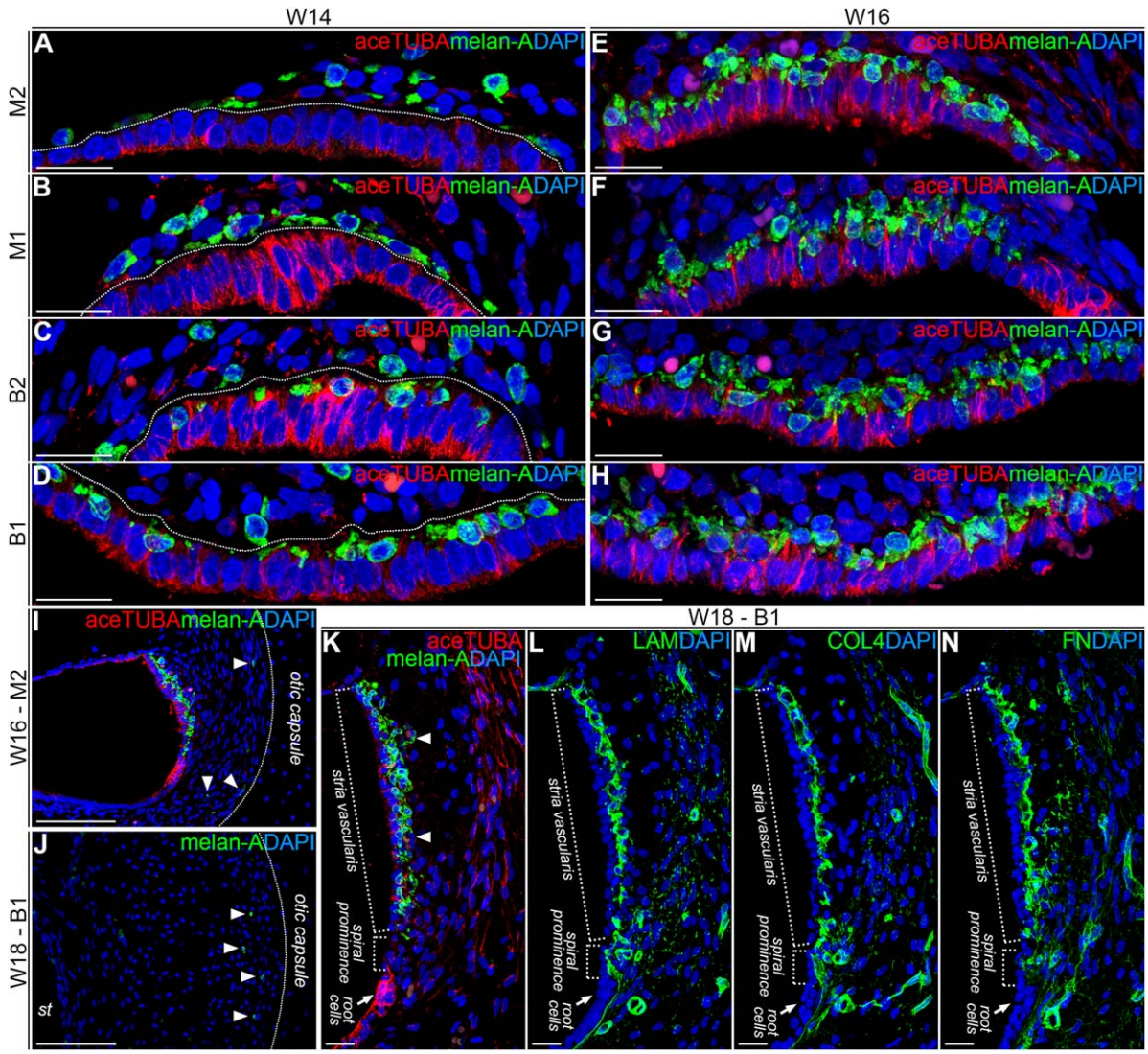

Figure 4 Maturation of the lateral wall in the human fetal cochlea. (A–D) Lateral wall area of the upper middle [M2, (A)], lower middle [M1, (B)], upper basal [B2, (C)], and lower basal [B1, (D)] turn of a cochlea at W14 immunostained for acetylated tubulin (aceTUBA; red), melan-A (green), and DAPI (blue). Scale bars = 20 μm. (E-H) Lateral wall area of the upper middle (E), lower middle (F), upper basal (G), and lower basal (H) turn of a cochlea at W16 immunostained for aceTUBA (red), melan-A (green), and DAPI (blue). Scale bars = 20 μm. (I) The upper middle turn of a cochlea at W16 immunostained for aceTUBA (red), melan-A (green), and DAPI (blue). Arrowheads point to melan-A+ melanocytes located in the periotic mesenchyme at the edges of the otic capsule. Scale bar = 100 μm. (J) The lower basal turn of a cochlea at W18 immunostained for melan-A (green) and DAPI (blue). Arrowheads point to melan-A+ melanocytes located in the periotic mesenchyme at the edges of the otic capsule. st = scala tympani. Scale bar = 100 μm. (K) The lower basal turn of a cochlea at W18 immunostained for aceTUBA (red), melan-A (green), and DAPI (blue). Arrowheads point to melan-A positive strial melanocytes around developing strial capillaries. Scale bar = 20 μm. (L–N) The lower basal turn of a cochlea at W18 immunostained for basement membrane proteins laminin (LAM) (L, green), collagen type IV (COL4) (M, green) and fibronectin (FN) (N, green), and DAPI (blue). Scale bars = 20 μm. [Color figure can be viewed in the online issue, which is available at wileyonlinelibrary.com.]

GJB6 (CX30, [MIM 604418]), GJA1 (CX43 [MIM 121014]), all known to be expressed in the human cochlea (Kammen-Jolly et al., 2001; Liu et al., 2009; Liu et al., 2013), and GJE1 (CX23 [MIM unknown]), which expression pattern has not been investigated previously in the cochlea (see Discussion).

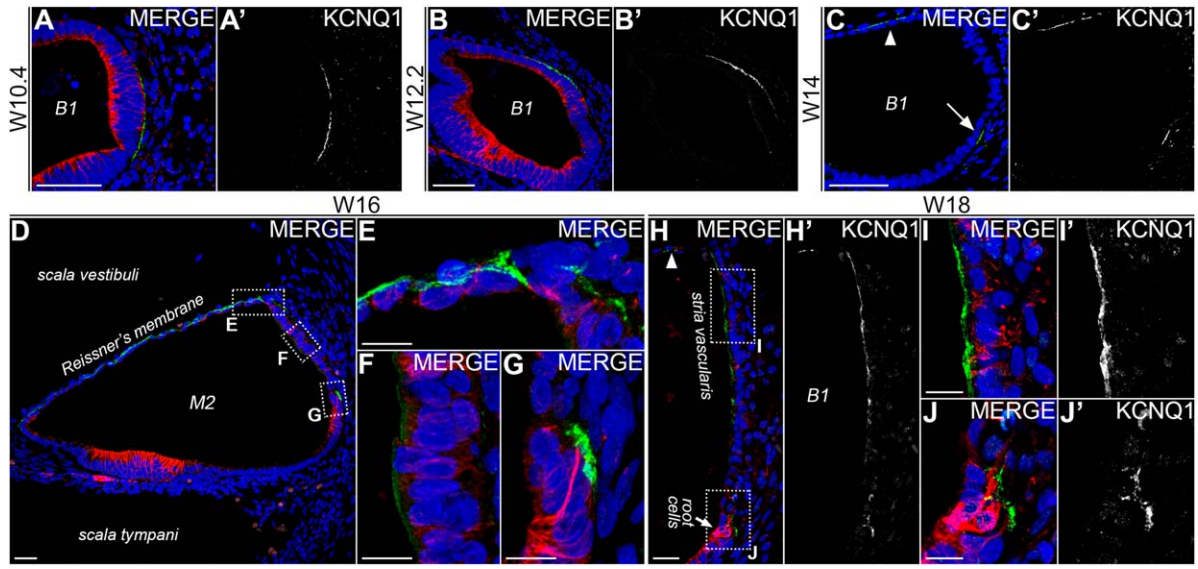

Figure 5 KCNQ1 expression in the human fetal cochlea. (A-A′) The lower basal turn of a cochlea at W10.4 immunostained for acetylated tubulin (aceTUBA) (red), voltage-gated potassium channel KCNQ1 (green), and DAPI (blue). The KCNQ1 signal is shown separately in white in (A′). Scale bar = 50 μm. (B-B′) The lower basal turn of a cochlea at W12.2 immunostained for aceTUBA (red), KCNQ1 (green), and DAPI (blue). The KCNQ1 signal is shown separately in white in (B′). Scale bar = 50 μm. (C-C′) The lower basal turn of a cochlea at W14 immunostained for aceTUBA (red), KCNQ1 (green), and DAPI (blue). The KCNQ1 signal is shown separately in (C′). The arrowhead points at KCNQ1 signals in the developing Reissner's membrane, the arrow points at KCNQ1 signals at the location of the future root cells. The KCNQ1 signal is shown separately in white in (C′). Scale bar = 50 μm. (D) The upper middle (M2) turn of a cochlea at W16 immunostained for aceTUBA (red), KCNQ1 (green), and DAPI (blue). Scale bar = 50 μm. (E–G) Higher magnifications of the outlined areas in (D), showing Reissner's membrane (E), the marginal cells of the stria vascularis (F), and the root cells in the outer sulcus (G). Scale bars = 20 μm. (H-H′) The lower basal turn of a cochlea at W18 immunostained for aceTUBA (red), KCNQ1 (green), and DAPI (blue). The arrowhead points to Reissner's membrane. The KCNQ1 signal is shown separately in white in (H′). Scale bar = 20 μm. (I-J′) Higher magnifications of the outlined areas in (H). KCNQ1 signals are shown separately in white in (I′) and (J′). Scale bars = 10 μm. [Color figure can be viewed in the online issue, which is available at wileyonlinelibrary.com.]

Throughout the investigated stages (W10.4–W18), the GJB2 and GJB6 expression patterns remained identical to each other (Fig. 8). At W10, immunostaining for GJB2 and for GJB6 showed a diffuse and punctated pattern in both Kolliker's organ and the cells of the future outer sulcus [Fig. 8(A,B)]. By W12, expression of GJB2 and GJB6 had greatly increased and could clearly be observed on both sides of the developing organ of Corti [Fig. 8(C,D)]. In the subsequent weeks, up to W18, this pattern remained consistent as both in the Kölliker's organ and in the cells lining the outer sulcus (Claudius' cells and future root cells) expression of GJB2 and GJB6 was observed [Fig. 8(E–J)]. Although expression of both GJB2 and GJB6 has been reported in the spiral ligament fibrocytes in the adult human cochlea (Liu et al., 2009), no expression could be observed in these cells at least up to W18 [Fig. 8(J)]. We also did not detect expression in the organ of Corti itself.

Immunostaining for GJA1 showed weak expression by a significant subgroup of spiral ligament fibrocytes at W14 [Fig. 9(A)]. In the subsequent weeks, this expression became more prominent and at W18 could be clearly defined as belonging to the type I fibrocytes [Fig. 9(B,C)].

Immunostaining for GJE1 revealed a dynamic pattern of expression during human cochlear development. At W10.4 and W12, strong expression of GJE1 was observed in the basolateral membranes of the future marginal cells [Fig. 10(A,B)]. Interestingly, at W14, expression was observed both in the lateral wall epithelium and in some of the cells in the adjacent periotic mesenchyme, presumably melanocytes [Fig. 10(C)]. At W16, expression of GJE1 was

downregulated by the developing marginal cells and became exclusively limited to those adjacent cells [Fig. 10(D)]. Double immunostaining at W18 for GJE1 and ATP1A1 confirmed the melanocytic origin of the signal, as no overlap in GJE1 and ATP1A1 was observed [Fig. 10(E,F)].

An overview of the observed spatiotemporal expression patterns of selected proteins in this study is presented in Table 2.

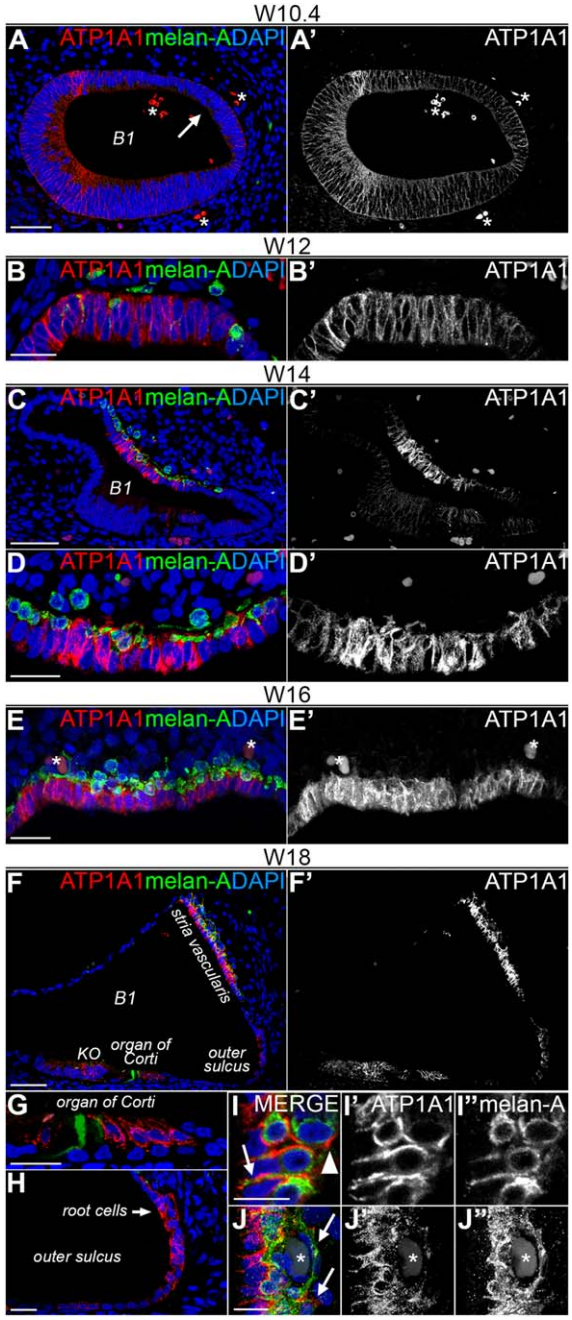

DISCUSSION

Are Human Cochlear Melanocytes Derived from the Neural Crest?

The developmental pattern of melanocyte distribution observed in the human fetal cochlea closely follows that of the mouse, where it is generally accepted that cochlear melanocytes are derived from the neural crest (Steel et al., 1992; Freyer et al., 2011; Wakaoka et al., 2013). Therefore, we suggest that the melanocytes in the human cochlea are also derived from the neural crest. However, in all species analyzed so far, the migratory route taken by melanocytes to arrive in the cochlea remains unknown. As cochlear development in humans progresses slower than in mice (as a rule of thumb, one day of rodent cochlear development corresponds to one week in humans), this

Figure 6 Expression of Na^+/K^+-ATPase in the human fetal cochlea. (A) The lower basal turn of a cochlea at W10.4 immunostained for Na^+/K^+-ATPase ATP1A1 (red), melan-A (green), and DAPI (blue). The arrow points to the location of the future stria vascularis. The ATP1A1 signal is shown separately in white in (A′). * = autofluorescent erythrocytes. Scale bar = 50 μm. (B) The lateral wall in the lower basal turn of a cochlea at W12 immunostained for ATP1A1 (red), melan-A (green), and DAPI (blue). The ATP1A1 signal is shown separately in white in (B′). Scale bar = 20 μm. (C) The lower basal turn of a cochlea at W14 immunostained for ATP1A1 (red), melan-A (green), and DAPI (blue). The ATP1A1 signal is shown separately in white in (C′). Scale bar = 50 μm. (D) Higher magnification of the developing stria vascularis in (C). The ATP1A1 signal is shown separately in white in (D′). Scale bar = 20 μm. (E) The developing stria vascularis in the lower basal turn of a cochlea at W16 immunostained for ATP1A1 (red), melan-A (green), and DAPI (blue). The ATP1A1 signal is shown separately in white in (E′). * = autofluorescent erythrocytes. Scale bar = 20 μm. (F) The lower basal turn of a cochlea at W18 immunostained for ATP1A1 (red), melan-A (green), and DAPI (blue). The ATP1A1 signal is shown separately in white in (F′). Scale bar = 50 μm. (G–H) Higher magnifications of (F), showing the organ of Corti (G) and epithelial lining of the outer sulcus (H). Scale bars = 20 μm. (I-J") Higher magnifications of the stria vascularis in (F), with the separate signals of ATP1A1 (I′ and J′) and melan-A (I" and J") shown in white. The arrow in (I) point to a melan-A+ melanocyte process penetrating toward the lumen of the cochlear duct. The arrowhead in (I) points toward an ATP1A1+ structure around a melan-A+ melanocyte cell body. The arrows in (J) point toward ATP1A1+ structures around melan-A+ processes that encircle a developing capillary. * = autofluorescent erythrocytes. Scale bars = 20 μm. [Color figure can be viewed in the online issue, which is available at wileyonlinelibrary.com.]

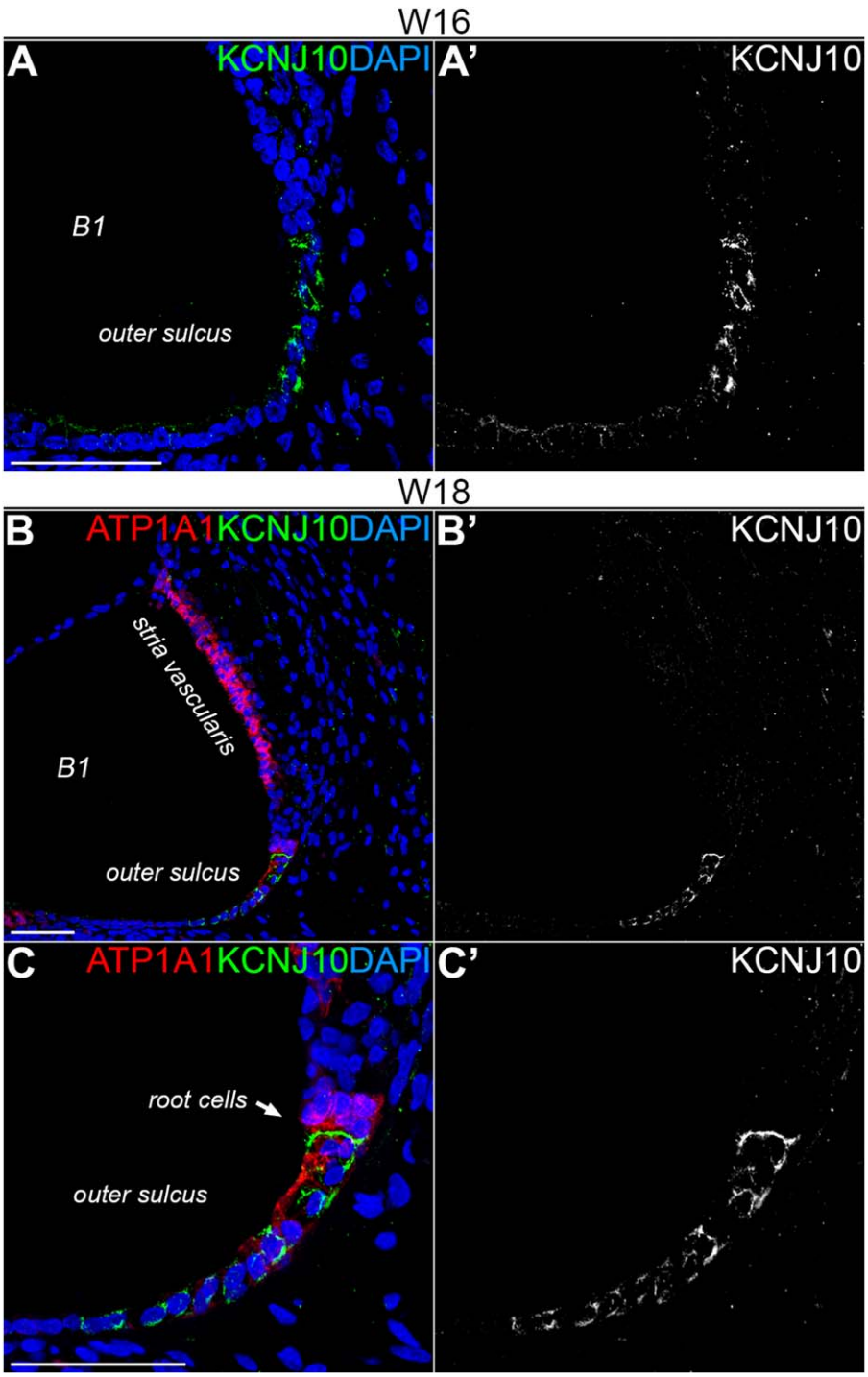

Figure 7 KCNJ10 expression in the human fetal cochlea. (A) The epithelial lining in the lower basal turn outer sulcus of a cochlea at W16 immunostained for the inwardly-rectifying potassium channel KCNJ10 (green) and DAPI (blue). The KCNJ10 signal is shown separately in white in (A′). Scale bar = 50 μm. (B) The lower basal turn of a cochlea at W18 immunostained for sodium/potassium-transporting ATPase ATP1A1 (red), KCNJ10 (green), and DAPI (blue). The KCNJ10 signal is shown separately in white in (B′). Scale bar = 50 μm. (C) Higher magnification of the outer sulcus area in (B). The KCNJ10 signal is shown separately in white in (C′). Scale bar = 50 μm. [Color figure can be viewed in the online issue, which is available at wileyonlinelibrary.com.]

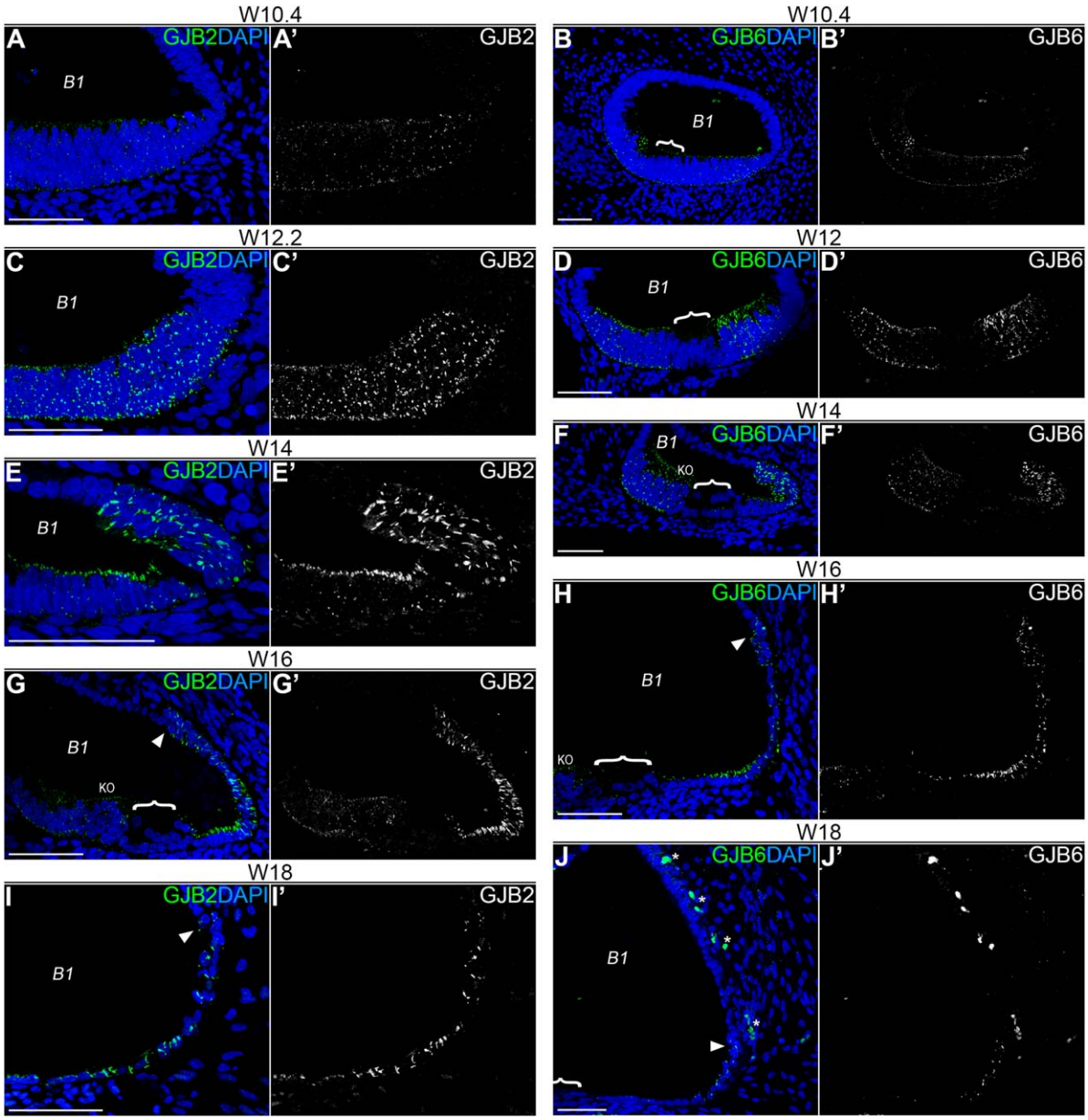

Figure 8 Epithelial expression of GJB2 and GJB6 in the cochlear duct. (A-B) The lower basal turn cochlea at W10.4 immunostained for gap junction proteins GJB2 [(A), green] and GJB6 [(B), green] and DAPI (blue). GJB2 and GJB6 signals are shown separately in white in (A′) and (B′), respectively. The bracket outlines the prosensory domain. Scale bars = 50 μm. (C-D) The lower basal turn cochlea at W12.2 immunostained for GJB2 [(C), green] and GJB6 [(D), green] and DAPI (blue). GJB2 and GJB6 signals are shown separately in white in (C′) and (D′), respectively. The bracket outlines the prosensory domain. Scale bars = 50 μm. (E-F) The lower basal turn cochlea at W14 immunostained for GJB2 ((E), green) and GJB6 ((F), green) and DAPI (blue). GJB2 and GJB6 signals are shown separately in white in (E′) and (F′), respectively. The bracket outlines the developing organ of Corti. KO = Kölliker's organ. Scale bars = 50 μm. (G–H) The lower basal turn cochlea at W14 immunostained for GJB2 [(G), green] and GJB6 [(H), green] and DAPI (blue). GJB2 and GJB6 signals are shown separately in white in (G′) and (H′), respectively. The arrowheads points to the developing root cells. The bracket outlines the developing of Corti. KO = Kölliker's organ. Scale bars = 50 μm. (I-J) The lower basal turn cochlea at W14 immunostained for GJB2 [(I), green] and GJB6 [(J), green] and DAPI (blue). GJB2 and GJB6 signals are shown separately in white in (I′) and (J′), respectively. The arrowheads points to the developing root cells. The bracket outlines the organ of Corti. * = autofluorescent erythrocytes. Scale bars = 50 μm. [Color figure can be viewed in the online issue, which is available at wileyonlinelibrary.com.]

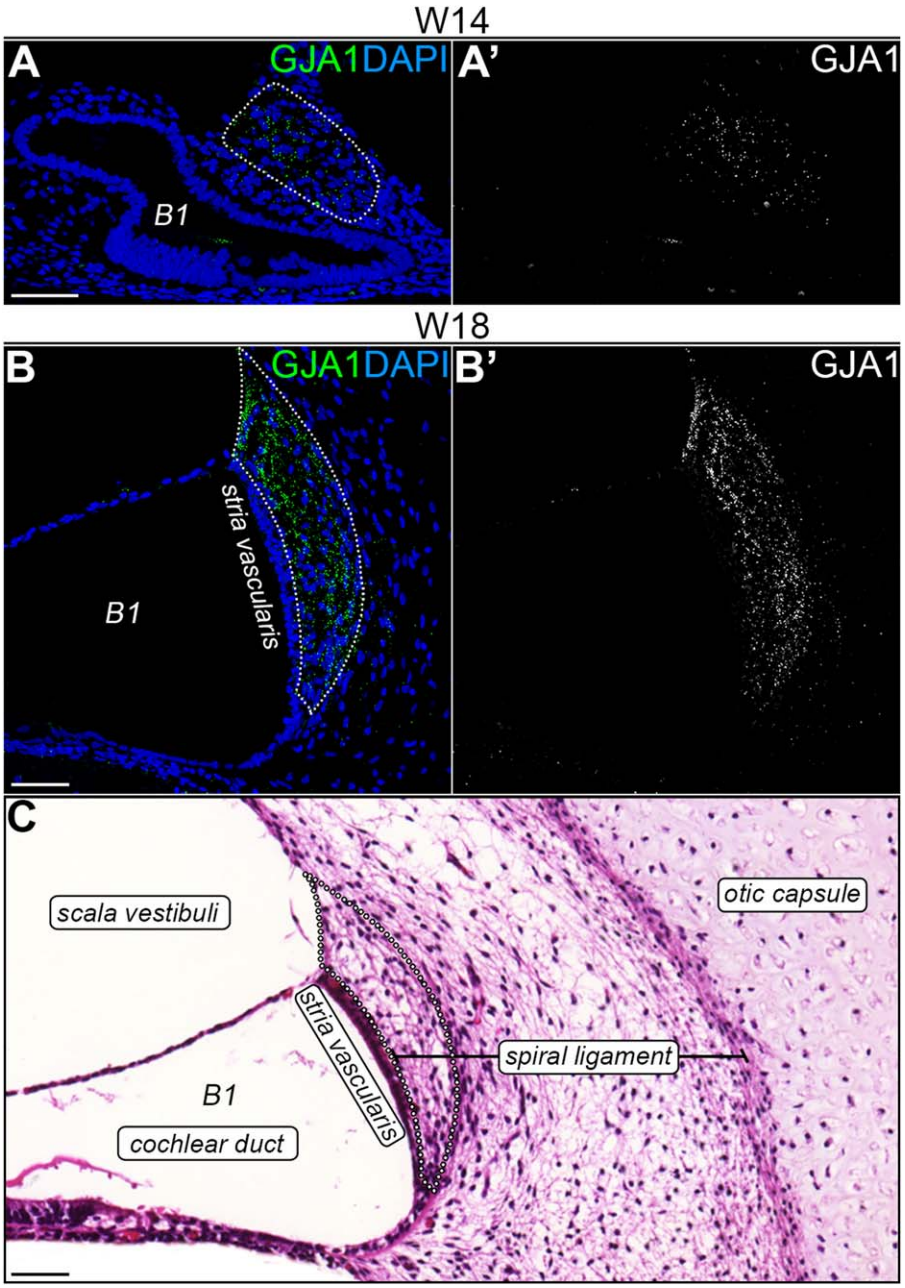

Figure 9 GJA1 is expressed by type I fibrocytes in the human fetal cochlea. (A) The lower basal turn of a cochlea at W14 immunostained for the gap junction protein GJA1 (green) and DAPI (blue). The dotted line outlines the group of spiral ligament fibrocytes expressing GJA1. The GJA1 signal is shown separately in white in (A′). Scale bar = 50 μm. (B) The lower basal turn of a cochlea at W18 immunostained for GJA1 (green) and DAPI (blue). The dotted line outlines the group of spiral ligament fibrocytes expressing GJA1. The GJA1 signal is shown separately in white in (B′). Scale bar = 50 μm. (C) Hematoxylin and eosin staining of a similar section as shown in (B). The dotted line represents the area of GJA1-expressing fibrocytes in (B). Scale bar = 50 μm. [Color figure can be viewed in the online issue, which is available at wileyonlinelibrary.com.]

permits a more explicit visualization of developmental events. Recently, it has been reported that cranial melanocytes can arise from Schwann cell precursors migrating together with outgrowing nerves (Adameyko et al., 2009; Adameyko et al., 2012). As Schwann cell precursors arrive in the cochlea via the cochlear nerve (Sandell et al., 2014), it is tempting to propose that melanocytes (precursors) may travel

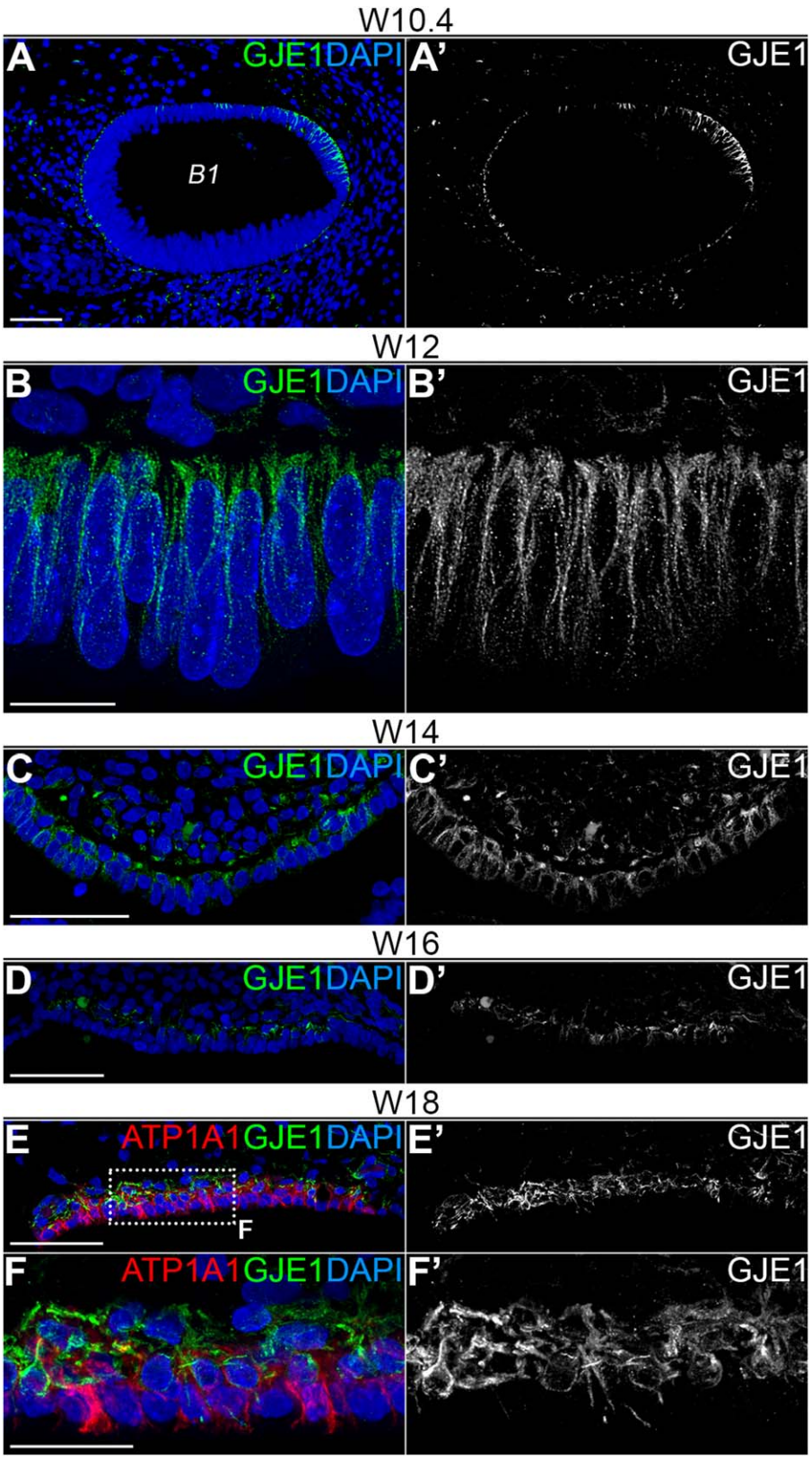
W10.4
A
GJE1DAPI
B1
A'
GJE1
W12
B
GJE1DAPI
B'
GJE1
W14
C
GJE1DAPI
C'
GJE1
W16
D
GJE1DAPI
D'
GJE1
W18
E
ATP1A1GJE1DAPI
F
E'
GJE1
F
ATP1A1GJE1DAPI
F'
GJE1

along the same path. However, our data on melanocyte migration toward their target location in the cochlea, which to our knowledge has not been shown before in such clarity, suggests that cochlear melanocytes in humans migrate through the periotic mesenchyme from the opposite side. In agreement, several studies in mice embryos show the presence of neural crest derivatives or melanocytes near this part of the otic vesicle around embryonic day 10.5 (Steel et al., 1992; Freyer et al., 2011; Adameyko et al., 2012; Wakaoka et al., 2013; Sandell et al., 2014). Therefore, although the peripheral glial cells in the cochlea originate from the migratory wave of neural crest cells from rhombomere 4, we now hypothesize that cochlear melanocytes originate from a different wave of neural crest cells, namely those delaminating from the region at rhombomere 6, at the location of the developing glossopharyngeal nerve (cranial nerve IX) and the third pharyngeal arch.

Cochlear Melanocytes, a Major Player in Syndromic SNHL

Intermediate cells in the stria vascularis were identified as melanocytes in 1977, although their exact function was unknown at that time (Hilding and Ginzberg, 1977). The involvement of cochlear melanocytes in generating the endocochlear potential was recognized later in a studies with "viable dominant spotting" mouse mutants, with a mutation in the *W* locus (Steel et al., 1987; Steel and Barkway, 1989). Shortly hereafter, *Kit* was found to be the gene product of the *W* locus (Chabot et al., 1988; Geissler et al., 1988), and it was shown to primarily affect the survival of migratory melanoblasts (Cable et al., 1995). In humans, *KIT* mutations can result in the neurocristopathy (a pathology affecting normal neural crest development) piebaldism [MIM 172800], a disorder characterized by areas of skin and hair devoid of melanocytes. Although most of these patients have a heterozygous mutation, deafness has been observed in rare cases of both heterozygous and homozygous mutations (Spritz and Beighton, 1998; Kilsby et al., 2013). We show that KIT is expressed by strial melanocytes in the human fetal cochlea, suggesting that SNHL due to *KIT* mutations in humans is caused by mechanisms similar to those in mouse *Kit* mutants.

Another neurocristopathy affecting melanocyte development with pigment abnormalities and SNHL is the genetically heterogeneous WS, the most common type of autosomal dominant SNHL in humans. Its four subtypes are based on clinical symptoms and multiple causative genes have been identified (Pingault et al., 2010). We show here that in the human fetal cochlea, MITF expression is confined to melanocytes [Fig. 3(A,C)]. Therefore, it is likely that cochlear melanocytes are responsible for SNHL in WS with *MITF* mutations (causing type IIa WS [MIM 193510]), and/or *PAX3* mutations (a gene regulating *MITF*, causative for type I WS [MIM 193500] and type III WS [MIM 148820]). In addition to *MITF*, mutations in *SOX10* can also cause type II WS in next to type IVc WS [MIM 613266] (Bondurand et al., 2007; Baral et al., 2012), whereas *SOX10* has recently also been identified to play a role in Kallmann syndrome with deafness (KS, [MIM 147950, 244200, 308700, 610628, 612370, and 612702]) (Pingault et al., 2013). SOX10 expression, however, is not exclusively limited to melanocytes in the human fetal cochlea [Fig. 3(B)]. We recently observed additional expression throughout the human fetal cochlear duct epithelium (Locher et al., 2013) and in all peripheral glial cells (Locher et al., 2014). Although it is likely that melanocytes play a major role in SNHL in WS or KS due to *SOX10* mutations, it cannot be excluded that other SOX10+ cell types in the cochlea are involved as well. Taken together, the melanocytic expression of MITF, SOX10, and KIT in the human fetal cochlea help to explain the

Figure 10 GJE1 expression dynamics during cochlear development in the human fetus. (A) The lower basal turn of a cochlea at W10.4 immunostained for the gap junction protein GJE1 (green) and DAPI (blue). The GJE1 signal is shown separately in white in (A′). Scale bar = 50 μm. (B) The developing stria vascularis in the lower basal turn of a cochlea at W12 immunostained for GJE1 (green) and DAPI (blue). The GJE1 signal is shown separately in white in (B′). Scale bar = 10 μm. (C) The developing stria vascularis in the lower basal turn of a cochlea at W14 immunostained for GJE1 (green) and DAPI (blue). The GJE1 signal is shown separately in white in (C′). Scale bar = 50 μm. (D) The developing stria vascularis in the lower basal turn of a cochlea at W16 immunostained for GJE1 (green) and DAPI (blue). The GJE1 signal is shown separately in white in (D′). Scale bar = 50 μm. (E) The developing stria vascularis in the lower basal turn of a cochlea at W18 immunostained for GJE1 (green) and DAPI (blue). The GJE1 signal is shown separately in white in (E′). Scale bar = 50 μm. (F) Higher magnification of the area outlined in (E). The GJE1 signal is shown separately in white in (F′). Scale bar = 20 μm.

Table 2 Spatiotemporal Expression Patterns of Investigated Proteins in the Developing Human Fetal Cochlea

Protein	Expression
SLC2A1 (GLUT1)	W12–W18: apical membrane of epithelial cells between organ of Corti and root cells in the outer sulcus (i.e. Hensen's cells, Claudius cells), capillaries, erythrocytes
ATP1A1	W10: throughout cochlear duct epithelium W12: increased expression in lateral wall epithelium W14–W18: basolateral membranes of marginal cells, basolateral membranes of inner and outer hair cells, basolateral membranes of epithelial cells in outer sulcus, Kölliker's organ.
KCNQ1 (KVLQT1)	W10–W12: basement membrane lateral wall epithelium W14: Reissner's membrane, developing root cells in outer sulcus W16–W18: apical membrane marginal cells, Reissner's membrane, developing root cells in outer sulcus
KCNJ10 ($K_{ir}4.1$)	W10–W14: no expression observed W16–W18: epithelial cells in outer sulcus, including root cells
GJB2 (CX26)	W10–W12: increased expression in epithelium of cochlear duct floor, with the exemption of the prosensory domain W14–W18: expression in Kölliker's organ and epithelial cells in outer sulcus
GJB6 (CX30)	Identical pattern to GJB2
GJA1 (CX43)	W10–W12: no expression observed W14–W18: increased expression in type I fibrocytes in the spiral ligament
GJE1 (CX23)	W10–W12: basolateral membranes of epithelial cells in lateral wall W14: basolateral membranes of marginal cells, melanocytes W16–W18: exclusive to melanocytes

aforementioned hereditary hearing disorders and underscore the important role of this cochlear cell type in syndromic SNHL.

The Endocochlear Potential and Its Relation to Hereditary SNHL

Hearing depends on the highly positive endocochlear potential, generated by the interplay of various ion channels and transporters in the cell types of the stria vascularis [reviewed in (Zdebik et al., 2009; Hibino et al., 2010)]. The location of these proteins along the membranes of the different cells of the adult stria vascularis is depicted in Figure 1(B). Disrupting the function of any of these proteins (including connexin proteins) in the stria vascularis or at other locations in the cochlea where they are thought to be involved in K^+ homeostasis results in immediate SNHL (Cohen-Salmon et al., 2002; Teubner et al., 2003; Nin et al., 2008). In many cases of both syndromic (as mentioned above) and nonsyndromic SNHL, the endocochlear potential is likely to be affected.

The marginal cells in the stria vascularis express the voltage-gated potassium channel KCNQ1 (or KCNE1, [MIM 176261]). Mutations in *KCNQ1* cause the autosomal recessive Jervell and Lange-Nielsen syndrome [MIM 220400], characterized by SNHL and cardiac abnormalities (long QT syndrome) (Jervell and Lange-Nielsen, 1957; Neyroud et al., 1997). In this syndrome, there is an impaired K^+ secretion into the endolymph by the KCNQ1/KCNE1 channel complex on the apical membranes of the marginal cells in the stria vascularis, as confirmed in a mouse model with the homozygous mutants being completely deaf (Lee et al., 2000). Since a low number of functional channels still result in normal hearing in heterozygous patients (Wollnik et al., 1997), it can be surmized that, to cause deafness, mutations in *KCNQ1* have to inactive the channel complex completely so that the total K^+-secretion is reduced to a minimum. On the basolateral membranes of the marginal cells, K^+ uptake from the intrastrial space (the narrow fluid-containing space between the marginal cells and the melanocytes) is mediated by the sodium-potassium pump Na^+/K^+-ATPase (Schulte and Adams, 1989) and the $Na^+2Cl^-K^+$ cotransporter. Na^+/K^+-ATPase is known to be expressed in the adult human stria vascularis (Weber et al., 2001) and inhibition of Na^+/K^+-ATPase directly suppresses the endocochlear potential in guinea pigs (Kuijpers and Bonting, 1970; Nin et al., 2008). We found first expression of KCNQ1 on the luminal membranes of the marginal cells at W16. At W18, we observed that the cell processes from the developing marginal cells

(expressing ATP1A1) and the strial melanocytes intermingle and form an intricate network together with the capillaries. The developmental expression of KCNQ1 and ATP1A1 indicates that both K^+ uptake and secretion could be mediated by marginal cells as early as W16–W18.

The pivotal role of strial melanocytes in the generation of the endocochlear potential is to secrete K^+ ions into the intrastrial space and hence they express the inward-rectifying potassium channel KCNJ10 (also known as $K_{ir}4.1$, [MIM 602208]) (Ando and Takeuchi, 1999; Eckhard et al., 2012). In contrast to the potassium channels of the marginal cells, we did not observe any KCNJ10 expression in strial melanocytes up to the last stage we investigated, W18. As inhibition of this receptor directly suppresses the endocochlear potential (Nin et al., 2008), it is likely that the endocochlear potential is not yet generated at this stage. *KCNJ10* is implicated in multiple syndromic disorders with SNHL. Loss-of-function mutations in *KCNJ10* cause SESAME syndrome ([MIM 612780], also called EAST syndrome), a disorder characterized by SNHL, electrolyte imbalance, seizures, ataxia and mental retardation. Here, the hearing loss is likely due to disrupted function of strial melanocytes (Scholl et al., 2009). *KCNJ10* is also implicated in SNHL in autosomal recessive deafness-4 (DFNB4) with enlarged vestibular aqueduct (EVA) [MIM 600791], and in autosomal recessive Pendred syndrome [MIM 274600]. In Pendred syndrome, *SLC26A4* [MIM 605646] mutations account for the majority of cases (Everett et al., 1997). The dysfunction of its protein, PENDRIN, results in loss of KCNJ10 expression in the melanocytes of the stria vascularis and subsequent loss of the endocochlear potential (Wangemann et al., 2004; Ito et al., 2014). However, mutations in *KCNJ10* itself have also been linked directly to Pendred syndrome (Yang et al., 2009). Interestingly, *KCNJ10* has also been described in the root cells of the outer sulcus, both in the adult rodent and human cochlea (Jagger et al., 2010; Eckhard et al., 2012). Also, the expression pattern of KCNJ10 that we observed in the outer sulcus during cochlear development matches the known expression pattern of PENDRIN in the outer sulcus of the adult mouse cochlea (Royaux et al., 2003; Wangemann et al., 2004). This provides a striking link between the two proteins and could help to explain the etiology of SNHL in Pendred syndrome.

Several connexins (Cx, gap junction proteins) are expressed at various locations in the cochlea and are thought to be implicated in K^+ recycling (Zdebik et al., 2009; Kelly et al., 2011). Mutations in connexins are a major cause of hereditary SNHL (Smith et al., 2014). The most frequent causative gene for nonsyndromatic SNHL is *GJB2* (*CX26*) (Smith et al., 2014). Although less frequent, mutations in *GJB6* (*CX30*) (Grifa et al., 1999; del Castillo et al., 2002) and *GJA1* (CX43) (Liu et al., 2001; Hong et al., 2010) have also been linked to SNHL. These gap junction proteins are thought to play a role in maintaining cochlear ion homeostasis and the endocochlear potential, as shown in *Gjb6*-deficient mice (Teubner et al., 2003), by passively recycling K^+ ions back to the stria vascularis. The observed expression in the developing human cochlea is in support of this model. However, an interesting note can be made with regard to the observed glucose transporter (SLC2A1) expression on the luminal membranes of the outer sulcus cells. As this part of the cochlea does not have its own vascularization, one could speculate that receptor expression at this luminal location functions to take up glucose circulating in the endolymph, suggesting a rather more active role for these cells with regard to cochlear K^+ homeostasis (with a potential role for the Na^+/K^+-ATPase?).

Finally, *GJE1* has not been previously investigated in the human cochlea. *GJE1* encodes the connexin 23 protein, and should not be confused with CX29/CX30.2, which used to be called *GJE1* but recently has been renamed to *GJC3* [MIM 611925]). In the developing human fetal cochlea, we observed dynamic GJE1 expression in the lateral wall, shifting from the developing marginal cells to the melanocytes between W14–W16. We speculate that *GJE1* could be a suitable candidate gene for non-syndromic SNHL, especially as a many causes of hereditary deafness remain presently unknown (Korver et al., 2011).

Maturation of the Lateral Wall and the Onset of Human Hearing

In many rodent species, development of hearing extends beyond birth and the onset of hearing occurs after birth (in an altricial manner). In contrast, hearing development in humans progresses at a much slower rate, but the cochlea and hearing function are complete before birth (precocial hearing development). Although cochlear size and degree of spiralization differs between species, the morphological appearance of the various cochlear tissues and structures as well as the subsequent protein expression profiles are very similar. Therefore, based on similarities in morphology and protein expression patterns in adult mammalian cochleas, we conclude that the human fetal cochlea at W18 demonstrates a nearly adult phenotype, but that some essential elements for functionality are still missing. Most notably, strial

melanocytes do not yet express KCNJ10, basal cells are immunohistochemically undefined, root cells have not developed their root-like basolateral processes, and GJB2 and GJB6 are not yet observed in the spiral ligament. This implies that the endocochlear potential cannot be generated at this stage and, therefore, that the human fetus at W18 is still unable to hear. Although W20 has been proposed by us (Locher et al., 2013; Locher et al., 2014) and others (Pujol et al., 1991; Pujol and Lavigne-Rebillard, 1995; Bibas et al., 2008) as the onset of human hearing based on the maturation of the organ of Corti and the cochlear nerve, it is more likely that hearing commences a few weeks later, which is in line with otoacoustic emission measurements (Chabert et al., 2006) and auditory brainstem responses in preterm infants (Lary et al., 1985; van Straaten et al., 2001).

In mice and gerbils, the appearance of the endocochlear potential has been observed just prior to their onset of hearing (Steel and Barkway, 1989; Souter and Forge, 1998), and coincides with morphological maturation of gap and tight junctions. Even although their auditory system does not become functional before birth, the sequence of morphological maturation is similar to what we observe in human fetuses. In view of these findings, extrapolation of our observations to later fetal stages suggests that the endocochlear potential, and therefore hearing, in the human fetus does not emerge before the third trimester of pregnancy.

CONCLUSION

We have investigated the complex embryonic development of the lateral wall in the human fetal cochlea with respect to the expression of several genes that are known to be involved both in syndromic and nonsyndromic SNHL, providing an etiological basis for these hearing disorders in humans. Although hereditary SNHL can be caused by specific mutations in various genes involved in cochlear K^+ transport, we would like to underline the major functional role of melanocytes in the cochlea and the generation of the endocochlear potential. We suggest that many cases of hereditary SNHL can be attributed to a disturbed development or migration of neural-crest-derived melanocytes.

ACKNOWLEDGMENTS

We would like to thank J. Wiegant and A.M. van der Laan for technical support, S.B. Blankevoort (anatomical, medical illustrator of the LUMC) for his work on Figure 1(A), and the Center for Contraception, Sexuality and Abortion (CASA) in Leiden and The Hague for the collection of the human fetal material.

REFERENCES

Adachi N, Yoshida T, Nin F, Ogata G, Yamaguchi S, Suzuki T, Komune S, et al. 2013. The mechanism underlying maintenance of the endocochlear potential by the K+ transport system in fibrocytes of the inner ear. J Physiol 591:4459–4472.

Adameyko I, Lallemend F, Aquino JB, Pereira JA, Topilko P, Müller T, Fritz N, et al. 2009. Schwann cell precursors from nerve innervation are a cellular origin of melanocytes in skin. Cell 139:366–379.

Adameyko I, Lallemend F, Furlan A, Zinin N, Aranda S, Kitambi SS, Blanchart A, et al. 2012. Sox2 and Mitf cross-regulatory interactions consolidate progenitor and melanocyte lineages in the cranial neural crest. Development 139:397–410.

Ando M, Takeuchi S. 1999. Immunological identification of an inward rectifier K+ channel (Kir4.1) in the intermediate cell (melanocyte) of the cochlear stria vascularis of gerbils and rats. Cell Tissue Res 298:179–183.

Angeli S, Lin X, Liu XZ. 2012. Genetics of hearing and deafness. Anat Rec (Hoboken) 295:1812–1829.

Baral V, Chaoui A, Watanabe Y, Goossens M, Attie-Bitach T, Marlin S, Pingault V, et al. 2012. Screening of MITF and SOX10 regulatory regions in Waardenburg syndrome type 2. PLoS One 7:e41927.

Bibas A, Liang J, Michaels L, Wright A. 2000. The development of the stria vascularis in the human foetus. Clin Otolaryngol Allied Sci 25:126–129.

Bibas AG, Xenellis J, Michaels L, Anagnostopoulou S, Ferekidis E, Wright A. 2008. Temporal bone study of development of the organ of Corti: Correlation between auditory function and anatomical structure. J Laryngol Otol 122:336–342.

Bizhanova A, Kopp P. 2010. Genetics and phenomics of Pendred syndrome. Mol Cell Endocrinol 322:83–90.

Bondurand N, Dastot-Le Moal F, Stanchina L, Collot N, Baral V, Marlin S, Attie-Bitach T, et al. 2007. Deletions at the SOX10 gene locus cause Waardenburg syndrome types 2 and 4. Am J Hum Genet 81:1169–1185.

Cable J, Jackson IJ, Steel KP. 1995. Mutations at the W locus affect survival of neural crest-derived melanocytes in the mouse. Mech Dev 50:139–150.

Chabert R, Guitton MJ, Amram D, Uziel A, Pujol R, Lallemant J-G, Puel J-L. 2006. Early maturation of evoked otoacoustic emissions and medial olivocochlear reflex in preterm neonates. Pediatr Res 59:305–308.

Chabot B, Stephenson DA, Chapman VM, Besmer P, Bernstein A. 1988. The proto-oncogene c-kit encoding a transmembrane tyrosine kinase receptor maps to the mouse W locus. Nature 335:88–89.

Cohen-Salmon M, Ott T, Michel V, Hardelin JP, Perfettini I, Eybalin M, Wu T, et al. 2002. Targeted ablation of

connexin26 in the inner ear epithelial gap junction network causes hearing impairment and cell death. Curr Biol 12:1106–1111.

Del Castillo I, Villamar M, Moreno-Pelayo MA, del Castillo FJ, Alvarez A, Tellería D, Menéndez I, et al. 2002. A deletion involving the connexin 30 gene in nonsyndromic hearing impairment. N Engl J Med 346:243–249.

Denoyelle F, Weil D, Maw MA, Wilcox SA, Lench NJ, Allen-Powell DR, Osborn a H, et al. 1997. Prelingual deafness: High prevalence of a 30delG mutation in the connexin 26 gene. Hum Mol Genet 6:2173–2177.

Eckhard A, Gleiser C, Rask-Andersen H, Arnold H, Liu W, Mack A, Müller M, et al. 2012. Co-localisation of K(ir)4.1 and AQP4 in rat and human cochleae reveals a gap in water channel expression at the transduction sites of endocochlear K(+) recycling routes. Cell Tissue Res 350:27–43.

Everett LA, Glaser B, Beck JC, Idol JR, Buchs A, Heyman M, Adawi F, et al. 1997. Pendred syndrome is caused by mutations in a putative sulphate transporter gene (PDS). Nat Genet 17:411–422.

Freyer L, Aggarwal V, Morrow BE. 2011. Dual embryonic origin of the mammalian otic vesicle forming the inner ear. Development 138:5403–5414.

Geissler EN, Ryan MA, Housman DE. 1988. The dominant-white spotting (W) locus of the mouse encodes the c-kit proto-oncogene. Cell 55:185–192.

Grifa A, Wagner CA, D'Ambrosio L, Melchionda S, Bernardi F, Lopez-Bigas N, Rabionet R, et al. 1999. Mutations in GJB6 cause nonsyndromic autosomal dominant deafness at DFNA3 locus. Nat Genet 23:16–18.

Hibino H, Nin F, Tsuzuki C, Kurachi Y. 2010. How is the highly positive endocochlear potential formed? The specific architecture of the stria vascularis and the roles of the ion-transport apparatus. Pflugers Arch 459:521–533.

Hilding DA, Ginzberg RD. 1977. Pigmentation of the stria vascularis. The contribution of neural crest melanocytes. Acta Otolaryngol 84:24–37.

Hilgert N, Smith RJH, Van Camp G. 2009a. Forty-six genes causing nonsyndromic hearing impairment: Which ones should be analyzed in DNA diagnostics? Mutat Res 681:189–196.

Hilgert N, Smith RJH, Van Camp G. 2009b. Function and expression pattern of nonsyndromic deafness genes. Curr Mol Med 9:546–564.

Hong H-M, Yang J-J, Shieh J-C, Lin M-L, Li M-L, Li S-Y. 2010. Novel mutations in the connexin43 (GJA1) and GJA1 pseudogene may contribute to nonsyndromic hearing loss. Hum Genet 127:545–551.

Hudspeth AJ. 1989. How the ear's works work. Nature 341:397–404.

Ito M, Spicer SS, Schulte BA. 1993. Immunohistochemical localization of brain type glucose transporter in mammalian inner ears: Comparison of developmental and adult stages. Hear Res 71:230–238.

Ito T, Li X, Kurima K, Choi BY, Wangemann P, Griffith AJ. 2014. Slc26a4-insufficiency causes fluctuating hearing loss and stria vascularis dysfunction. Neurobiol Dis 66:53–65.

Jagger DJ, Nevill G, Forge A. 2010. The membrane properties of cochlear root cells are consistent with roles in potassium recirculation and spatial buffering. J Assoc Res Otolaryngol 448:435–448.

Jervell A, Lange-Nielsen F. 1957. Congenital deaf-mutism, functional heart disease with prolongation of the Q-T interval and sudden death. Am Heart J 54:59–68.

Kammen-Jolly K, Ichiki H, Scholtz AW, Gsenger M, Kreczy A, Schrott-Fischer A. 2001. Connexin 26 in human fetal development of the inner ear. Hear Res 160: 15–21.

Kelly JJ, Forge A, Jagger DJ. 2011. Development of gap junctional intercellular communication within the lateral wall of the rat cochlea. Neuroscience 180:360–369.

Kelsell DP, Dunlop J, Stevens HP, Lench NJ, Liang JN, Parry G, Mueller RF, et al. 1997. Connexin 26 mutations in hereditary non-syndromic sensorineural deafness. Nature 387:80–83.

Kilsby AJ, Cruwys M, Kukendrajah C, Russell-Eggitt I, Raglan E, Rajput K, Loshe P, et al. 2013. Homozygosity for piebaldism with a proven KIT mutation resulting in depigmentation of the skin and hair, deafness, developmental delay and autism spectrum disorder. Clin Dysmorphol 22:64–67.

Kim SH, Kim KX, Raveendran NN, Wu T, Pondugula SR, Marcus DC. 2009. Regulation of ENaC-mediated sodium transport by glucocorticoids in Reissner's membrane epithelium. Am J Physiol Cell Physiol 296:C544–C557.

Kimura RS, Schuknecht HF. 1970. The ultrastructure of the human stria vascularis. I. Acta Otolaryngol 69:415–427.

Korver AMH, Admiraal RJC, Kant SG, Dekker FW, Wever CC, Kunst HPM, Frijns JHM, et al. 2011. Causes of permanent childhood hearing impairment. Laryngoscope 121:409–416.

Kuijpers W, Bonting SL. 1970. The cochlear potentials. I. The effect of ouabain on the cochlear potentials of the guinea pig. Pflugers Arch 320:348–358.

Lary S, Briassoulis G, de Vries L, Dubowitz LM, Dubowitz V. 1985. Hearing threshold in preterm and term infants by auditory brainstem response. J Pediatr 107:593–599.

Lavigne-Rebillard M, Bagger-Sjöbäck D. 1992. Development of the human stria vascularis. Hear Res 64:39–51.

Lee MP, Ravenel JD, Hu RJ, Lustig LR, Tomaselli G, Berger RD, Brandenburg S a, et al. 2000. Targeted disruption of the Kvlqt1 gene causes deafness and gastric hyperplasia in mice. J Clin Invest 106:1447–1455.

Linden Phillips L, Bitner-Glindzicz M, Lench N, Steel KP, Langford C, Dawson SJ, Davis A, et al. 2013. The future role of genetic screening to detect newborns at risk of childhood-onset hearing loss. Int J Audiol 52:124–133.

Liu W, Boström M, Kinnefors A, Rask-Andersen H. 2009. Unique expression of connexins in the human cochlea. Hear Res 250:55–62.

Liu W, Glueckert R, Linthicum FH, Rieger G, Blumer M, Bitsche M, Pechriggl E, et al. 2014. Possible role of gap junction intercellular channels and connexin 43 in

satellite glial cells (SGCs) for preservation of human spiral ganglion neurons : A comparative study with clinical implications. Cell Tissue Res 355:267–278.

Liu XZ, Xia XJ, Adams J, Chen ZY, Welch KO, Tekin M, Ouyang XM, et al. 2001. Mutations in GJA1 (connexin 43) are associated with non-syndromic autosomal recessive deafness. Hum Mol Genet 10:2945–2951.

Locher H, de Groot JCMJ, van Iperen L, Huisman MA, Frijns JHM, Chuva de Sousa Lopes SM. 2013. Neurosensory development and cell fate determination in the human cochlea. Neural Dev 8:20.

Locher H, Frijns JHM, van Iperen L, de Groot JCMJ, Huisman MA, Chuva de Sousa Lopes SM. 2014. Distribution and development of peripheral glial cells in the human fetal cochlea. B. Sokolowski, ed. PLoS One 9: e88066.

Morton CC, Nance WE. 2006. Newborn hearing screening–a silent revolution. N Engl J Med 354:2151–2164.

Neyroud N, Tesson F, Denjoy I, Leibovici M, Donger C, Barhanin J, Fauré S, et al. 1997. A novel mutation in the potassium channel gene KVLQT1 causes the Jervell and Lange-Nielsen cardioauditory syndrome. Nat Genet 15: 186–189.

NHSP. 2011. Annual Report NHS Newborn Hearing Screening Programme, 2010–2011.

Nin F, Hibino H, Doi K, Suzuki T, Hisa Y, Kurachi Y. 2008. The endocochlear potential depends on two K+ diffusion potentials and an electrical barrier in the stria vascularis of the inner ear. Proc Natl Acad Sci USA 105: 1751–1756.

Patuzzi R. 2011. Ion flow in stria vascularis and the production and regulation of cochlear endolymph and the endolymphatic potential. Hear Res 277:4–19.

Pendred V. 1896. Daef-mutism and Goitre. Lancet 148: 532.

Pingault V, Bodereau V, Baral V, Marcos S, Watanabe Y, Chaoui A, Fouveaut C, et al. 2010. Review and update of mutations causing Waardenburg syndrome. Hum Mutat 31:391–406.

Pingault V, Ente D, Dastot-Le Moal F, Goossens M, Marlin S, Bondurand N. 2013. Loss-of-function mutations in SOX10 cause Kallmann syndrome with deafness. Am J Hum Genet 92:707–724.

Pujol R, Lavigne-Rebillard M. 1995. Sensory and neural structures in the developing human cochlea. Int J Pediatr Otorhinolaryngol 32:S177–S182.

Pujol R, Lavigne-Rebillard M, Uziel A. 1991. Development of the human cochlea. Acta Otolaryngol Suppl 482:7–12; discussion 13.

Royaux IE, Belyantseva IA, Wu T, Kachar B, Everett LA, Marcus DC, Green ED. 2003. Localization and functional studies of pendrin in the mouse inner ear provide insight about the etiology of deafness in Pendred syndrome. J Assoc Res Otolaryngol 4:394–404.

Sandell LL, Butler Tjaden NE, Barlow AJ, Trainor PA. 2014. Cochleovestibular nerve development is integrated with migratory neural crest cells. Dev Biol 385:200–210.

Schindelin J, Arganda-Carreras I, Frise E, Kaynig V, Longair M, Pietzsch T, Preibisch S, et al. 2012. Fiji: An open-source platform for biological-image analysis. Nat Methods 9:676–682.

Scholl UI, Choi M, Liu T, Ramaekers VT, Häusler MG, Grimmer J, Tobe SW, et al. 2009. Seizures, sensorineural deafness, ataxia, mental retardation, and electrolyte imbalance (SeSAME syndrome) caused by mutations in KCNJ10. Proc Natl Acad Sci USA 106:5842–5847.

Schulte BA, Adams JC. 1989. Distribution of immunoreactive Na+,K+-ATPase in gerbil cochlea. J Histochem Cytochem 37:127–134.

Shearer EA, Smith RJH. 2012. Genetics: Advances in genetic testing for deafness. Curr Opin Pediatr 24:679–686.

Smith CA, Lowry OH, Wu ML. 1954. The electrolytes of the labyrinthine fluids. Laryngoscope 64:141–153.

Smith RJ, Shearer AE, Hildebrand MS, van Camp G. 2014. Deafness and Hereditary Hearing Loss Overview. GeneReviewsTM [Internet] http://www.ncbi.nlm.nih.gov/books/NBK1434/. Accessed on February 2014.

Souter M, Forge A. 1998. Intercellular junctional maturation in the stria vascularis: Possible association with onset and rise of endocochlear potential. Hear Res 119:81–95.

Spritz RA, Beighton P. 1998. Piebaldism with deafness: Molecular evidence for an expanded syndrome. Am J Med Genet 75:101–103.

Steel KP, Barkway C. 1989. Another role for melanocytes: Their importance for normal stria vascularis development in the mammalian inner ear. Development 107:453–463.

Steel KP, Barkway C, Bock GR. 1987. Strial dysfunction in mice with cochleo-saccular abnormalities. Hear Res 27: 11–26.

Steel KP, Davidson DR, Jackson IJ. 1992. TRP-2/DT, a new early melanoblast marker, shows that steel growth factor (c-kit ligand) is a survival factor. Development 115:1111–1119.

Stelma F, Bhutta MF. 2014. Non-syndromic hereditary sensorineural hearing loss: Review of the genes involved. J Laryngol Otol 128:13–21.

Teubner B, Michel V, Pesch J, Lautermann J, Cohen-Salmon M, Söhl G, Jahnke K, et al. 2003. Connexin30 (Gjb6)-deficiency causes severe hearing impairment and lack of endocochlear potential. Hum Mol Genet 12:13–21.

van Camp G, Smith RJ. 2014. Hereditary Hearing Loss Homepage, http://hereditaryhearingloss.org/. Accessed on February, 2014.

van der Ploeg CPB, Uilenburg NN, Kauffman-de Boer MA, Oudesluys-Murphy AM, Verkerk PH. 2012. Newborn hearing screening in youth health care in the Netherlands: National results of implementation and follow-up. Int J Audiol 51:584–590.

van Straaten HL, Tibosch CH, Dorrepaal C, Dekker FW, Kok JH. 2001. Efficacy of automated auditory brainstem response hearing screening in very preterm newborns. J Pediatr 138:674–678.

Waardenburg PJ. 1951. A new syndrome combining developmental anomalies of the eyelids, eyebrows and nose

root with pigmentary defects of the iris and head hair and with congenital deafness. Am J Hum Genet 3:195–253.

Wakaoka T, Motohashi T, Hayashi H, Kuze B, Aoki M, Mizuta K, Kunisada T, et al. 2013. Tracing Sox10-expressing cells elucidates the dynamic development of the mouse inner ear. Hear Res 302:17–25.

Wangemann P, Itza EM, Albrecht B, Wu T, Jabba S V, Maganti RJ, Lee JH, et al. 2004. Loss of KCNJ10 protein expression abolishes endocochlear potential and causes deafness in Pendred syndrome mouse model. BMC Med 2:30.

Weber PC, Cunningham CD, Schulte BA. 2001. Potassium recycling pathways in the human cochlea. Laryngoscope 111:1156–1165.

WHO. 2014. Fact Sheet No300.

Wollnik B, Schroeder BC, Kubisch C, Esperer HD, Wieacker P, Jentsch TJ. 1997. Pathophysiological mechanisms of dominant and recessive KVLQT1 K+ channel mutations found in inherited cardiac arrhythmias. Hum Mol Genet 6:1943–1949.

Yang T, Gurrola JG, Wu H, Chiu SM, Wangemann P, Snyder PM, Smith RJH. 2009. Mutations of KCNJ10 together with mutations of SLC26A4 cause digenic non-syndromic hearing loss associated with enlarged vestibular aqueduct syndrome. Am J Hum Genet 84:651–657.

Zdebik AA, Wangemann P, Jentsch TJ. 2009. Potassium ion movement in the inner ear: Insights from genetic disease and mouse models. Physiology (Bethesda) 24:307–316.